Cell Reports

Article

Human iPSC-derived renal collecting duct organoid model cystogenesis in ADPKD

Graphical abstract

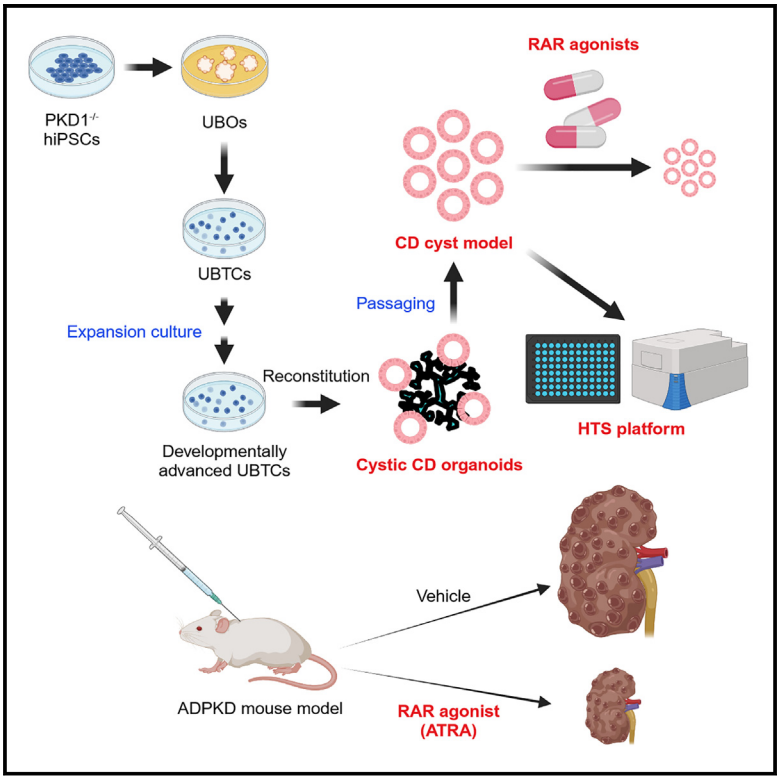

Highlights

- Expanded UB tip cells can be differentiated into cortical collecting duct (CD) cells
- *In vitro* CD cystogenesis model is established from ADPKD-specific iPSCs
- RAR agonists significantly suppress cyst enlargement in the *in vitro* CD cystogenesis model
- ATRA has therapeutic effects on an ADPKD mouse model *in vivo*

Authors

Shin-Ichi Mae, Fumihiko Hattanda, Hiroyoshi Morita, ..., Tomoyoshi Soga, Saori Nishio, Kenji Osafune

Correspondence

osafu@cira.kyoto-u.ac.jp

In brief

Mae et al. induced cortical-cell-containing collecting duct (CD) organoids from hiPSCs and developed an *in vitro* CD cystogenesis model of ADPKD. They also identified that RAR agonists suppress cyst enlargement using the *in vitro* model and confirmed the therapeutic effect on an ADPKD mouse model *in vivo*.

Mae et al., 2023, Cell Reports *42*, 113431
December 26, 2023
https://doi.org/10.1016/j.celrep.2023.113431

CellPress

Cell Reports

CellPress
OPEN ACCESS

Article

Human iPSC-derived renal collecting duct organoid model cystogenesis in ADPKD

Shin-Ichi Mae,[1] Fumihiko Hattanda,[2] Hiroyoshi Morita,[1] Aya Nozaki,[1] Naoko Katagiri,[1] Hanako Ogawa,[3] Kaori Teranaka,[3] Yu Nishimura,[3] Aoi Kudoh,[4] Sanae Yamanaka,[5] Kyoko Matsuse,[1] Makoto Ryosaka,[1] Akira Watanabe,[3,4] Tomoyoshi Soga,[5] Saori Nishio,[2] and Kenji Osafune[1,6,*]

[1]Center for iPS Cell Research and Application (CiRA), Kyoto University, 53 Kawahara-cho, Shogoin, Sakyo-ku, Kyoto 606-8507, Japan
[2]Department of Rheumatology, Endocrinology and Nephrology, Faculty of Medicine and Graduate School of Medicine, Hokkaido University, Kita-15 Nishi-7, Kita-ku, Sapporo, Hokkaido 060-8638, Japan
[3]CyberomiX Co., Ltd., 233 Isa-cho, Kamigyo-ku, Kyoto 602-8407, Japan
[4]Medical Innovation Center, Graduate School of Medicine, Kyoto University, 53 Kawahara-cho, Shogoin, Sakyo-ku, Kyoto 606-8507, Japan
[5]Institute for Advanced Bioscience, Keio University, 246-2 Mizukami, Kakuganji, Tsuruoka, Yamagata 997-0052, Japan
[6]Lead contact
*Correspondence: osafu@cira.kyoto-u.ac.jp
https://doi.org/10.1016/j.celrep.2023.113431

SUMMARY

In autosomal dominant polycystic kidney disease (ADPKD), renal cyst lesions predominantly arise from collecting ducts (CDs). However, relevant CD cyst models using human cells are lacking. Although previous reports have generated *in vitro* renal tubule cyst models from human induced pluripotent stem cells (hiPSCs), therapeutic drug candidates for ADPKD have not been identified. Here, by establishing expansion cultures of hiPSC-derived ureteric bud tip cells, an embryonic precursor that gives rise to CDs, we succeed in advancing the developmental stage of CD organoids and show that all CD organoids derived from *PKD1*$^{-/-}$ hiPSCs spontaneously develop multiple cysts, clarifying the initiation mechanisms of cystogenesis. Moreover, we identify retinoic acid receptor (RAR) agonists as candidate drugs that suppress *in vitro* cystogenesis and confirm the therapeutic effects on an ADPKD mouse model *in vivo*. Therefore, our *in vitro* CD cyst model contributes to understanding disease mechanisms and drug discovery for ADPKD.

INTRODUCTION

Autosomal dominant polycystic kidney disease (ADPKD) causes the progressive formation of numerous renal cysts and leads to end-stage renal failure that requires dialysis therapy or kidney transplantation.[1] This disorder is the most frequent among monogenic disorders, affecting approximately one in 1,000 individuals, and is responsible for 5%–10% of kidney failure worldwide.[2] It has been reported that renal cysts in patients with ADPKD predominantly arise from collecting ducts (CDs), although glomerular and renal tubular epithelia also develop cyst lesions.[3] Tolvaptan, an antagonist of arginine vasopressin receptor 2 (AVPR2), which is specifically expressed in CDs, is the only clinically approved drug for ADPKD, but it does not control the disease progression. Therefore, relevant CD cystogenesis models that reproduce the human ADPKD pathology are needed.

Organoids that recapitulate many key features of the represented organs can significantly improve disease models in a dish. Several studies have reported renal tubule cyst models using nephron organoids derived from ADPKD-specific human pluripotent stem cells (hPSCs).[4–9] However, although a chemical compound that suppresses cyst formation *in vitro* was identified using these models, the therapeutic effects of the drug on ADPKD animal models *in vivo* have not been shown.[7] Other reports have generated CD organoids from hPSCs,[9–12] but these organoids do not reach the developmentally advanced stages that express key molecules involved in CD cyst formation in ADPKD, such as AVPR2.[1] Furthermore, no reports have reproduced the spontaneous cyst formation of ADPKD or the therapeutic effects of tolvaptan using CD organoids.

Self-renewing stem cells that can differentiate into multiple cell types to reproduce the spatiotemporal organization of the corresponding organs are present in organoids.[13] During development of the renal collecting system, the progenitor tissue, ureteric bud (UB), repeats branching morphogenesis to form a tree-like structure containing two distinct domains, the tip and the trunk. In this process, the tip produces a new tip and trunk, demonstrating that the tip acts as stem cells.[14] Recently, we succeeded in efficiently differentiating human induced PSCs (hiPSCs) into branching UB organoids (UBOs) and subsequently generated UB tip cell (UBTC) colonies from dissociated single UBO cells that can reconstitute UBOs (Figure S1).[10]

In the present study, we established a long-term expansion culture method for UBTCs that advances their developmental stage to develop cortical-cell-containing CD organoids (Figure S1). Importantly, UBTCs derived from ADPKD-specific hiPSCs differentiated into CD organoids that spontaneously developed cysts after the developmental stage of UBTCs progressed, and the cyst formation was inhibited by tolvaptan. We

further reduced cystogenesis by identifying several biochemical signals that activate cyst formation, including lipid-metabolism-related signals. Moreover, by developing a mass production method for CD cysts using the passage culture, we established a high-throughput screening (HTS) platform that explores therapeutic drug candidates for ADPKD. In the process of establishing this platform, we identified retinoic acid receptor (RAR) agonists as candidate drug compounds for suppressing cyst enlargement in our established *in vitro* ADPKD model and successfully confirmed the therapeutic effects of all-*trans* retinoic acid (ATRA) on an ADPKD mouse model *in vivo*. Since no reports have shown the therapeutic effects of RAR agonists on ADPKD, and since ATRA is a clinically used drug,[15] these findings may substantially contribute to drug discovery for ADPKD.

RESULTS

Modification of the previously reported expansion culture method for UBTCs

We found that the weekly passaged UBTC colonies, which were generated through UBOs from a normal hiPSC line, 1231A3,[16] by our previously reported method,[10] gradually decreased in size and lost the ability to reconstitute UBOs and to express a UBTC-specific marker gene, *WNT11* (data not shown; Figure S2A). Consistent with previous reports on mouse UB,[17,18] we confirmed the endogenous expression of *TGFβ2* in UBOs and the inhibition of branching by transforming growth factor β2 (TGF-β2; 10 ng/mL; Figures S2B and S2C). We also found that the addition of 1 μM of a TGF-β signal inhibitor, A83-01, promoted branching and increased the proportion of UBTCs in UBOs, as evaluated by the DiI-VLDL uptake we reported previously[10] (Figures S2D and S2E), indicating that the inhibition of TGF-β signaling supports UBTC proliferation. Accordingly, we modified the UBTC generation method from UBOs by adding 1 μM A83-01 (Figures 1A–1D). We also found that the addition of A83-01 enhances the proliferation of passaged UBTCs (Figure 1E) and maintains *WNT11* expression (Figure 1F). After 4 weeks of weekly passage culture with A83-01, the colonies maintained UBTC marker expression (Figures 1G and 1H) and were able to reconstitute UBOs (Figure 1I). Importantly, stocked UBTCs with a commercially available cryopreservation reagent also maintained the potential to reconstitute UBOs (Figure S2F). Thus, we used these cryopreserved cells in most of the following experiments (Table S1).

To elucidate the mechanisms of UBTC expansion, we performed RNA sequencing (RNA-seq) and compared 4-week-cultured UBTCs with or without A83-01. The expression of several UB trunk markers, including *WNT9B* and *FOXA1*, and stromal markers, including *MEIS1*, *MEIS2*, *COL3A1*, and *POSTN*, was upregulated in UBTCs cultured without A83-01 (Figure 1J). In contrast, A83-01-treated UBTCs showed an enrichment of gene sets such as "tumor necrosis factor α [TNF-α] signaling via nuclear factor κB [NF-κB]" and "interleukin-6 [IL-6] JAK STAT3 signaling" (Figure 1K), which is consistent with mouse UB.[19] The inhibition of NF-κB signaling with an inhibitor of IκBα phosphorylation, BAY 11-7082 (2 μM), suppressed the proliferation of UBTCs (Figures 1L and 1M). Moreover, the addition of BAY 11-7082 inhibited the branching of UBOs (Figure S2G). These results indicate that NF-κB signaling is crucial for UBTC proliferation.

Advancement of UB development

After 6 weeks of UBTC expansion culture, the cell proliferation rate was decreased (Figure 2A), although UBTCs still retained the ability to import DiI-VLDL (Figure 2B). Long-term-expanded UBTCs derived from three different normal hiPSC lines, 1231A3, 1383D2, and 1383D6,[16] also showed a reduced proliferation rate but with the ability to reconstitute UBOs (Figure 2C) with repeated bifurcate branching (Figure 2D). Further differentiation with an additional 7 day CD induction using previously reported factors, 1 μM of a Wnt pathway inhibitor, IWR-1, 1 μM A83-01, and 10 μM of a cAMP signaling activator, forskolin, instead of vasopressin,[10,11] induced $AQP2^+$ CD principal cells from both 2- and 6-week-cultured UBTCs (Figure 2E), suggesting that the long-term expansion culture changes the properties of UBTCs that are independent of organoid reconstitution and CD differentiation.

During mouse UB development, *Sall4* and *Kit* are expressed until the early branching phase,[20,21] while *Lcn2* expression is enhanced at the late branching phase.[22,23] RNA-seq showed that 2-week-cultured UBTCs highly expressed *SALL4* and *KIT* but that *LCN2* expression was upregulated in 6-week-cultured UBTCs (Figure 2F). Interestingly, 6-week-cultured UBTCs also showed an enhanced expression of a cellular senescence marker, *CDKN2A* (Figure 2F). The upregulated enriched gene sets in 6-week-cultured UBTCs were "inflammatory response" and "TNF-α signaling via NF-κB" (Figure S2H) and included *IL1B* and *CCL20*, markers for senescence-associated secretory phenotype (SASP) (Figure 2F).[24] In addition, the enhancement of the gene sets "apoptosis" and "p53 pathway" may reflect slower cell growth of UBTCs at the late branching phase (Figure S2H).

We predicted the ability of UBTCs to differentiate into cortical CD tissues is acquired after long-term expansion culture. To test this hypothesis, we conducted a single-cell RNA-seq (scRNA-seq) analysis of CD organoids generated from 2- and 6-week-cultured UBTCs that were further differentiated with the additional 7 day CD induction described above by dimensionality reduction to cluster cells in the organoids with similar gene expression profiles using uniform manifold approximation and projection (UMAP). We determined 13 clusters and found that most contain *AQP2*-expressing CD cells (clusters 0, 1, 2, 3, 6, 7, 9, and 11) (Figures S3A and S3B). By performing a reference mapping of the scRNA-seq dataset using the previously reported Azimuth toolkit,[25] we found that our CD organoids were comprised of not only inner medullary CD (IMCD) cells but also of papillary tip epithelial cells, outer medullary CD (OMCD) principal cells, cortical CD (CCD) principal cells, and connecting tubule cells (Figure 2G). To strengthen the significance of our findings, we integrated our scRNA-seq datasets with the dataset of CD organoids from a recent report (GEO: GSE206153)[12] (Figure S3C) and analyzed the identities of the cells in each CD organoid (Figure S3D). Although IMCD cells are dominant in all three CD organoids, the proportion of CCD principal cells was slightly higher in CD organoids differentiated from 6-week-cultured UBTCs than those from 2-week-cultured UBTCs (Table S2). In

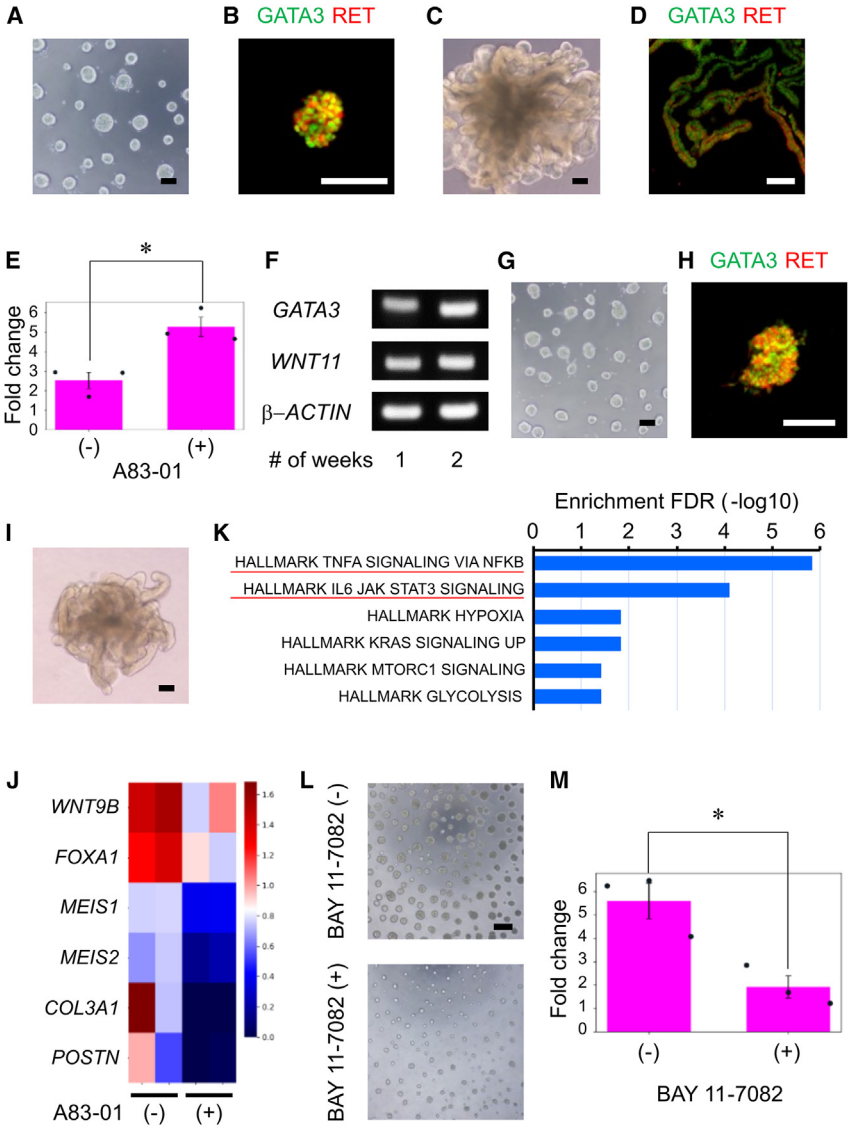

Figure 1. Establishment of an expansion culture method for UBTCs

(A and B) Morphology (A) and immunostaining analysis for GATA3 (green) and RET (red; B) of 1-week-cultured UBTCs that were generated from dissociated single UBO cells with 1 μM A83-01.

(C and D) Morphology (C) and immunostaining analysis for GATA3 (green) and RET (red; D) of day 14 UBOs reconstituted from 1-week-cultured UBTCs.

(E) The fold changes in the number of UBTCs from 1 to 2 weeks with or without 1 μM A83-01 were 5.23 ± 0.85 and 2.52 ± 0.72, respectively. Data are from three independent experiments and are presented as the mean ± SD (n = 3).

(F) An RT-PCR analysis of marker genes for UB tips in UBTCs cultured for 1 and 2 weeks with 1 μM A83-01.

(G and H) Morphology (G) and immunostaining analysis for GATA3 (green) and RET (red; H) of 4-week-cultured UBTCs.

(I) Morphology of a day 14 UBO reconstituted from 4-week-cultured UBTCs.

(J) A heatmap showing differentially expressed genes between 4-week-cultured UBTCs with or without A83-01 evaluated by RNA-seq.

(K) An enrichment analysis of genes upregulated in A83-01-treated UBTCs. All pathways with GSEA false discovery rate (FDR) <0.05 are shown.

(L) Morphology of 2-week-cultured UBTCs (top). Adding 2 μM BAY 11-7082 to the UBTCs suppressed the proliferation (bottom).

(M) The fold changes in the number of UBTCs from 1 to 2 weeks with or without 2 μM BAY 11-7082 were 1.92 ± 0.84 and 5.60 ± 1.32, respectively. Data are from three independent experiments and are presented as the mean ± SD (n = 3). *p < 0.05 by Student's t test. Scale bars, 100 μm. All data were obtained from 1231A3-hiPSCs.

contrast, there were no CCD principal cells in the previously reported CD organoids (Table S2).[12] We then performed a trajectory analysis using Monocle2 and found that in the pseudotime axis, a heatmap roughly divided the first 1,000 differentially expressed genes (DEGs) into two clusters (Figure S3E). Using the Metascape bioinformatics tool, we found that genes highly expressed on the left side of the heatmap (clusters 2, 5, and 6) were characteristic of CCD, whereas genes on the right side (clusters 1, 3, and 4) were enriched in medullary CD (MCD), suggesting transcriptional dynamics during the CD organoid formation (data not shown; Table S3). Upon comparing IMCD cells generated from 2- and 6-week-cultured UBTCs, we found that the expression of *AQP3*, a marker of IMCD,[26] is higher in CD organoids differentiated from 6-week-cultured UBTCs than those from 2-week-cultured UBTCs (Figure S4A; Table S4). In addition, since another recent report showed the importance of metabolic changes for the advancement of kidney development,[27] the up-regulation of the gene set related to "aerobic glycolysis" in 6-week-cultured-UBTC-derived IMCD cells compared to 2-week-cultured-UBTC-derived IMCD cells indicated that IMCD cells from the 6-week-cultured UBTCs are more developmentally advanced (Figure S4B). CCD cells derived from 6-week-cultured UBTCs showed an enrichment of gene sets such as "the citric acid (TCA) cycle and respiratory electron transport" compared to those from 2-week-cultured UBTCs (Figure 2H; Table S4). Because the importance of glucose as the main energy source decreases as CD progresses to the cortex from the inner medulla,[28] the change in the metabolic signature suggests the advanced differentiation of CCDs from 6-week-cultured UBTCs. Therefore, we concluded that the long-term expansion culture of UBTCs advances their developmental stage to the late branching phase in association with cellular senescence. To clearly distinguish UB/CD lineage organoids along developmental stages, we hereafter refer to the reconstituted organoids from expanded UBTCs as "cortical cell-containing CD organoids." Interestingly, we also found that ATP6V1B1^{+} intercalated cells (ICs) are generated

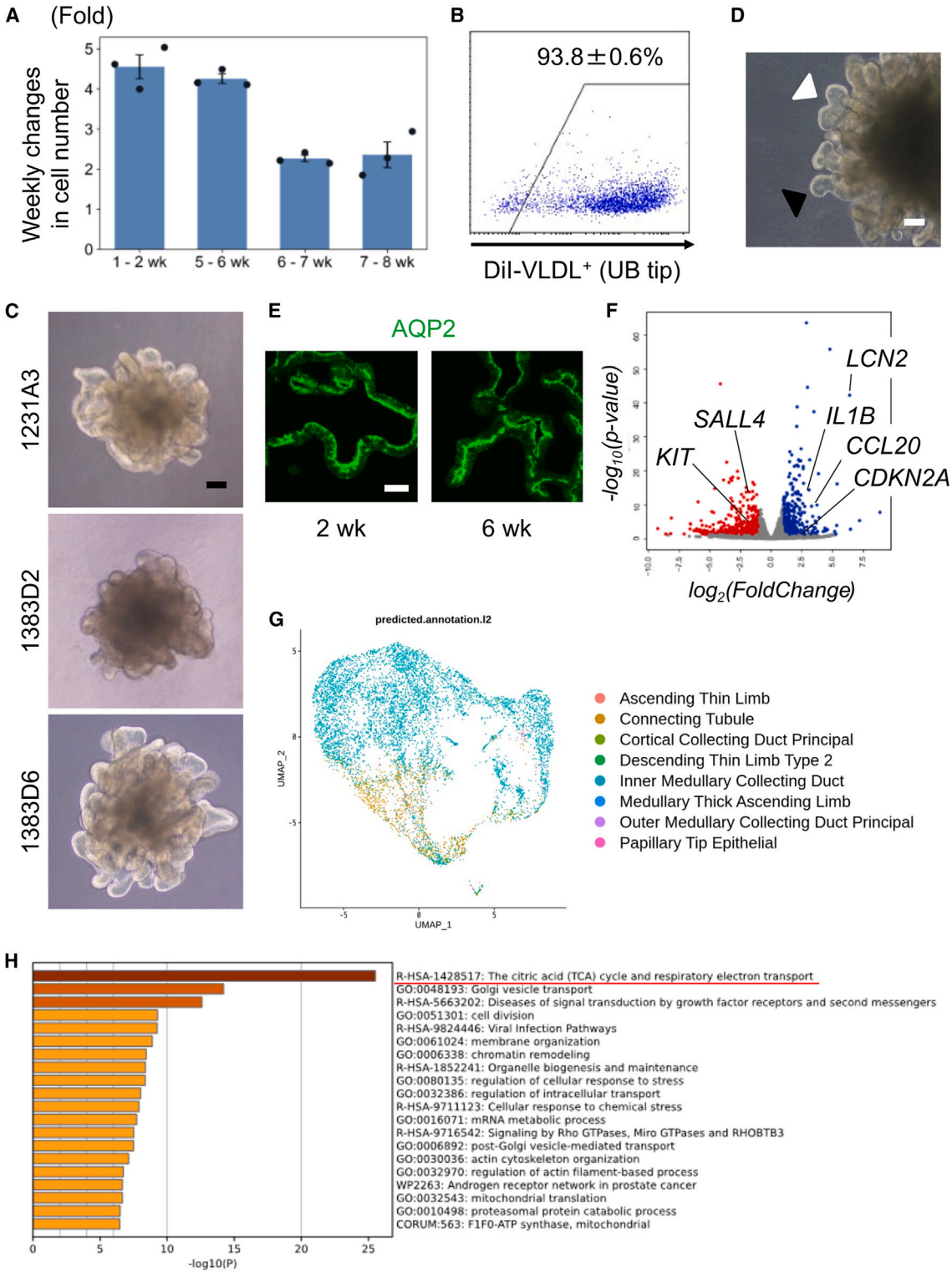

Figure 2. Long-term expansion culture of UBTCs

(A) The weekly change in the number of UBTCs.

(B) The percentage of DiI-VLDL$^+$ cells in 7-week-cultured UBTCs based on flow cytometry analysis.

(C) Morphology of day 14 UBOs reconstituted from 8-week-cultured UBTCs that were differentiated from three different hiPSC lines (1231A3, 1383D2, and 1383D6).

(legend continued on next page)

from 3-week-cultured UBTCs but hardly from 6-week-cultured UBTCs (Figure S4C; data not shown).

Development of an *in vitro* ADPKD model

Mouse embryos with Pkd1 homozygous mutations develop progressive CD cysts from the late branching phase of UB.[29] Therefore, we hypothesized that if the mechanisms of mouse renal development are conserved in human, CD cyst formation can be recapitulated by generating CD tissues from UBTCs with homozygous PKD1 mutations at the corresponding developmental stage. Using a homozygous PKD1-mutant (*PKD1*$^{-/-}$) hiPSC line that we previously established from another normal hiPSC line, 585A1,[30] using the CRISPR-Cas9 system,[8] we examined cyst formations in cortical-cell-containing CD organoids reconstituted from the late branching phase of *PKD1*$^{-/-}$ hiPSC-derived UBTCs. As expected, spontaneous cyst formations gradually occurred in cortical-cell-containing CD organoids derived from UBTCs after 6 week or longer expansion culture (Figure 3A), whereas parental *PKD1*$^{+/+}$ hiPSC-derived cortical-cell-containing CD organoids did not form any cysts (Figure 3B). All cortical-cell-containing CD organoids from 8-week-cultured *PKD1*$^{-/-}$ UBTCs spontaneously formed numerous cysts (data not shown). Next, we generated additional *PKD1*$^{-/-}$ hiPSC lines from two different parental hiPSC lines, 1231A3 and 1383D2, using the CRISPR-Cas9 system[31] (Figure S5A). We found that all these *PKD1*$^{-/-}$ hiPSC-line-derived cortical-cell-containing CD organoids spontaneously formed cysts (Figure S5B). However, the severity of the cyst formation depended on the cell line, and cystogenesis occurred in cortical-cell-containing CD organoids from even 4-week-cultured UBTCs that were differentiated from *PKD1*$^{-/-}$ 1383D2-hiPSCs (Figure S5C; data not shown). Therefore, we used cortical-cell-containing cystic CD organoids induced from *PKD1*$^{-/-}$ 1383D2-hiPSCs in the following experiments.

We found that the cyst cells were positive for a proliferation marker, Ki67, and a cyst cell marker, N-CADHERIN[32] (Figure 3C). Notably, the cysts were considered to have the properties of CD because they also expressed a CD marker, CK19, instead of RET (Figure 3C). The activation of cAMP signaling is a key growth mechanism of cyst cells.[1] We confirmed that forskolin treatment significantly promoted cyst enlargement in our model (Figures 3D and 3E), whereas *PKD1*$^{+/+}$ cortical-cell-containing CD organoids did not form cysts by this treatment (Figure S5D). The increased number of Ki67^{+} cells suggested that the proliferation of cyst cells enhances cyst enlargement (Figure S5E). We also found that forskolin-treated enlarged cysts express two mature CD markers, AQP2 and AVPR2, and a cilia marker, ARL13B, although AVPR2 was expressed on the apical side or in cytoplasm only (Figures 3F and 3G).

Characterization of cyst cells

To identify triggers of cystogenesis, we examined 6-week-cultured UBTCs that spontaneously form cysts. An RNA-seq analysis indicated that cilia-related genes were altered in *PKD1*$^{-/-}$ UBTCs (Figure S6A), suggesting that *PKD1* mutation caused the cilia malfunction since the *PKD1* gene product, polycystin 1, is expressed on cilia.[1] Then, we used the Metascape bioinformatics tool and identified liver-specific genes as enriched in *PKD1*$^{-/-}$ UBTCs (Figure S6B), which is consistent with previous reports that show the upregulation of liver-specific genes, such as *HNF4α* and *FOXA2*, in renal cysts from patients with ADPKD[33] and in mouse cystic kidneys with the loss of polycystin 1 or polycystin 2.[34] Taken together, the upregulation of liver-specific genes might promote cystogenesis.

A gene set enrichment analysis (GSEA) showed that crucial signals for UBTC expansion including "TNF-α signaling via NF-κB" and "inflammatory response" are downregulated in *PKD1*$^{-/-}$ UBTCs (Figures 1K, S2H, and S6C), while the cell-cycle-related signals "E2F target" and "G2M checkpoint" are enriched in *PKD1*$^{-/-}$ UBTCs (Figure 4A), suggesting that the suppression of SASP leads to the enhancement of cell proliferation. Notably, in *PKD1*$^{-/-}$ UBTCs, anaerobic-glycolysis-related terms, including "mTORC1 signaling," "hypoxia," and "glycolysis" were decreased, while "oxidative phosphorylation" was enhanced (Figure S7A), which is consistent with a recent report that found that the TCA cycle is significantly altered in the initiation of cyst formation.[35] Moreover, "fatty acid metabolism," including *CD36* and β-oxidation-related genes, was upregulated in *PKD1*$^{-/-}$ UBTCs (Figures S7B and S7C). The elevated intracellular ATP levels in *PKD1*$^{-/-}$ UBTCs suggest that extracellular fatty acid uptake is enhanced to promote ATP production (Figure 4B). Interestingly, cholesterol-metabolism-related terms, including "cholesterol homeostasis" and "bile acid metabolism," were enhanced in *PKD1*$^{-/-}$ UBTCs (Figure 4C). Metabolome analysis showed that intracellular lipid levels, including cholesterol, were also increased in *PKD1*$^{-/-}$ UBTCs (Figure S8). Statins that inhibit cholesterol production are used as an effective treatment for lipid metabolism disorders,[36] and the effects of statins on ADPKD have been investigated in recent years.[37,38] Thus, we examined the effects of fluvastatin in our cystogenesis model and found that cyst formation was significantly suppressed in cortical-cell-containing CD organoids reconstituted from fluvastatin-treated UBTCs (Figure 4D), although the addition of fluvastatin in the reconstitution step of the CD organoids from UBTCs inhibited the organoids formation (data not shown).

Next, by comparing cyst cells and CD cells in cortical-cell-containing cystic CD organoids after 7 days of further CD

(D) Morphology of day 21 UBOs reconstituted from 6-week cultured UBTCs. Outgrowth (black arrowhead) and bifurcate branching (white arrowhead) of UB are indicated.

(E) Immunostaining of day 21 CD organoids after 7 day CD maturation treatment of day 14 UBOs reconstituted from 2- or 6-week-cultured UBTCs for AQP2 (green).

(F) A volcano plot showing differentially expressed genes between 2- and 6-week-cultured UBTCs evaluated by RNA-seq.

(G) Reference mapping of the scRNA-seq dataset from CD organoids that were differentiated from 2- and 6-week-cultured UBTCs using the Azimuth toolkit.

(H) An enrichment analysis of genes upregulated in CCD principal cells differentiated from 6-week-cultured UBTCs compared with those from 2-week-cultured UBTCs. Enriched terms with $p < 0.01$ are shown.

Scale bars, 100 μm in (C) and (D) and 50 μm in (E). All data except (C) were obtained from 1231A3-hiPSCs.

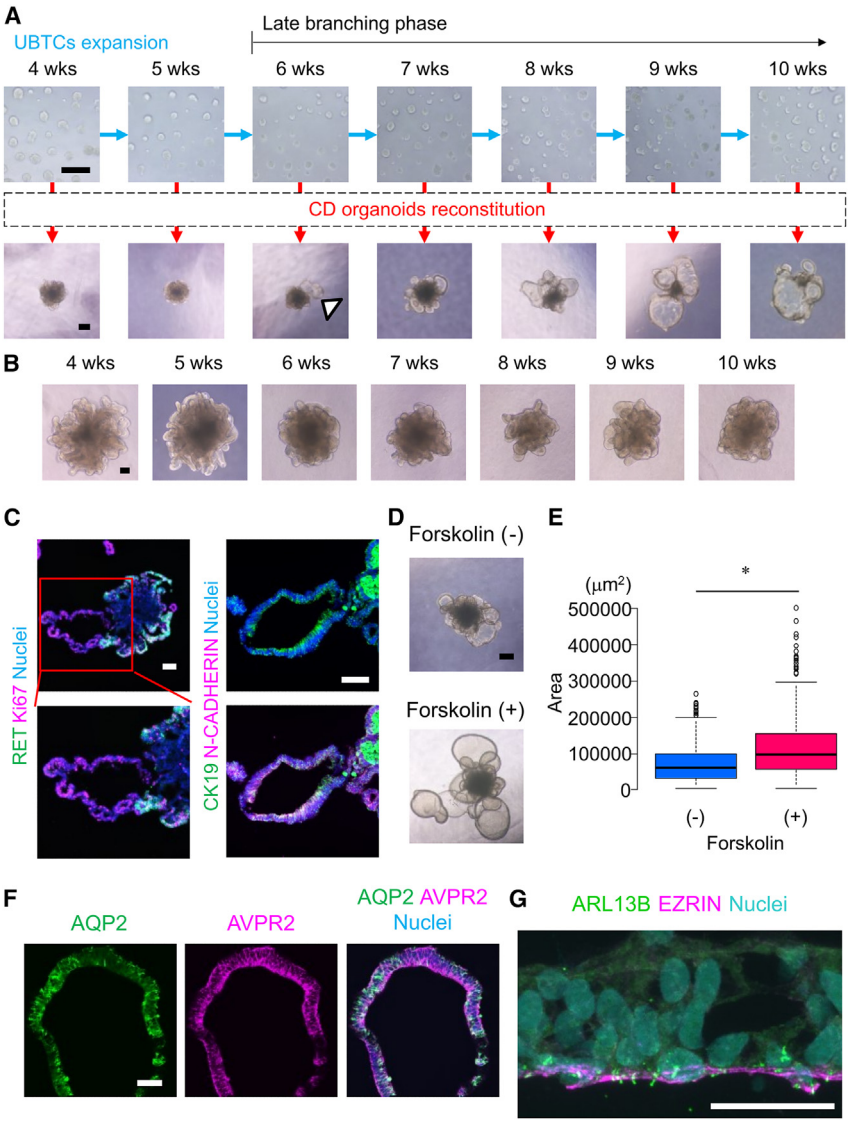

Figure 3. Development of a spontaneous CD cystogenesis model

(A) Morphology of UBTCs that were differentiated from *PKD1*$^{-/-}$ 585A1-hiPSCs after 4 to 10 weeks of weekly expansion culture (top) and day 14 CD organoids reconstituted from the corresponding UBTCs (bottom). The arrowhead indicates cyst structures in a CD organoid reconstituted from 6-week-cultured UBTCs. Note that the severity of the spontaneous cyst formation in CD organoids gradually increased as the developmental stage progressed after the late branching phase.

(B) Morphology of day 14 CD organoids reconstituted from the corresponding UBTCs that were differentiated from *PKD1*$^{+/+}$ 585A1-hiPSCs after 4 to 10 weeks of weekly expansion culture.

(C) Immunostaining of day 14 cyst-containing CD organoids reconstituted from 4-week-cultured UBTCs that were differentiated from *PKD1*$^{-/-}$ 1383D2-hiPSCs for RET (green), Ki67 (purple), and nuclei (blue; left) and for CK19 (green), N-CADHERIN (purple), and nuclei (blue; right). A magnified image of the boxed area in the top left is shown in the bottom left.

(D) Morphology of day 14 CD organoids reconstituted from 7-week-cultured *PKD1*$^{-/-}$ 1383D2-derived UBTCs and cultured with or without 10 μM forskolin for an additional 4 days.

(E) Cyst size with (n = 471) or without (n = 604) 10 μM forskolin. *p < 0.001 by Mann-Whitney U test. Data are from three independent experiments and are presented as the mean ± SD.

(F) Immunostaining of a day 7 cyst-containing CD organoid reconstituted from 6-week-cultured UBTCs and treated with 10 μM forskolin for an additional 5 days for AQP2 (green), AVPR2 (purple), and nuclei (blue).

(G) Immunostaining of a day 7 cyst-containing CD organoid reconstituted from 4-week-cultured UBTCs and treated with 10 μM forskolin for an additional 5 days for ARL13B (green), EZRIN (purple), and nuclei (blue).

Scale bars, 100 μm in (A)–(D), 50 μm in (F), and 20 μm in (G). All data except (A) and (B) were obtained from *PKD1*$^{-/-}$ 1383D2-hiPSCs.

induction, we found that N-CADHERIN^{+} cyst cells expressed AQP2, although the expression was weaker than in CDs (Figure 4E). Since cyst cells also expressed AVPR2, they were considered to have mature CD-like characteristics. The RNA-seq analysis of UBTCs also revealed that HNF4α and SOX2 expression can distinguish cysts from CDs (Figure 4E).

Development of an HTS platform

To develop HTS platforms, it is necessary to average the number and size of cysts, which vary among organoids. Accordingly, we developed a passage culture method for CD cysts by enzymatic dissociation and culture without adding forskolin (Figures 5A and 5B). In addition, to screen chemical compounds that suppress cyst enlargement, it is crucial to shorten the period of the cyst structure formation, which takes 10 days from single cyst cells. We found that forskolin treatment accelerates cyst formation from single cyst cells and shortens the period to 2 days and that the cysts continued to expand without shrinking even after the withdrawal of forskolin (Figures 5C and 5D).

Next, we examined whether AVP treatment enhances cyst enlargement because it activates cAMP signaling and promotes cyst cell proliferation.[1] A significant increase in cyst size was observed when 2.5 μM AVP was added during cyst formation (Figures 5E and 5F). We also found that 5 μM tolvaptan significantly suppressed cyst enlargement and proliferation by AVP (Figures 5G and S9A). The apoptosis cell rate was not changed, and the expression of AVPR2 was retained after tolvaptan treatment (Figure S9A). These data suggest that tolvaptan is a useful positive control for HTS. Then, we confirmed that using 200–300 cysts per compound makes the effects of variation in individual cyst size minimal and established a 96-well-based HTS platform (Figure S9B; see STAR Methods). Using the platform, we evaluated the efficacy of three compounds that have been tested in clinical trials for ADPKD.[1] Treatment with a glucosylceramide

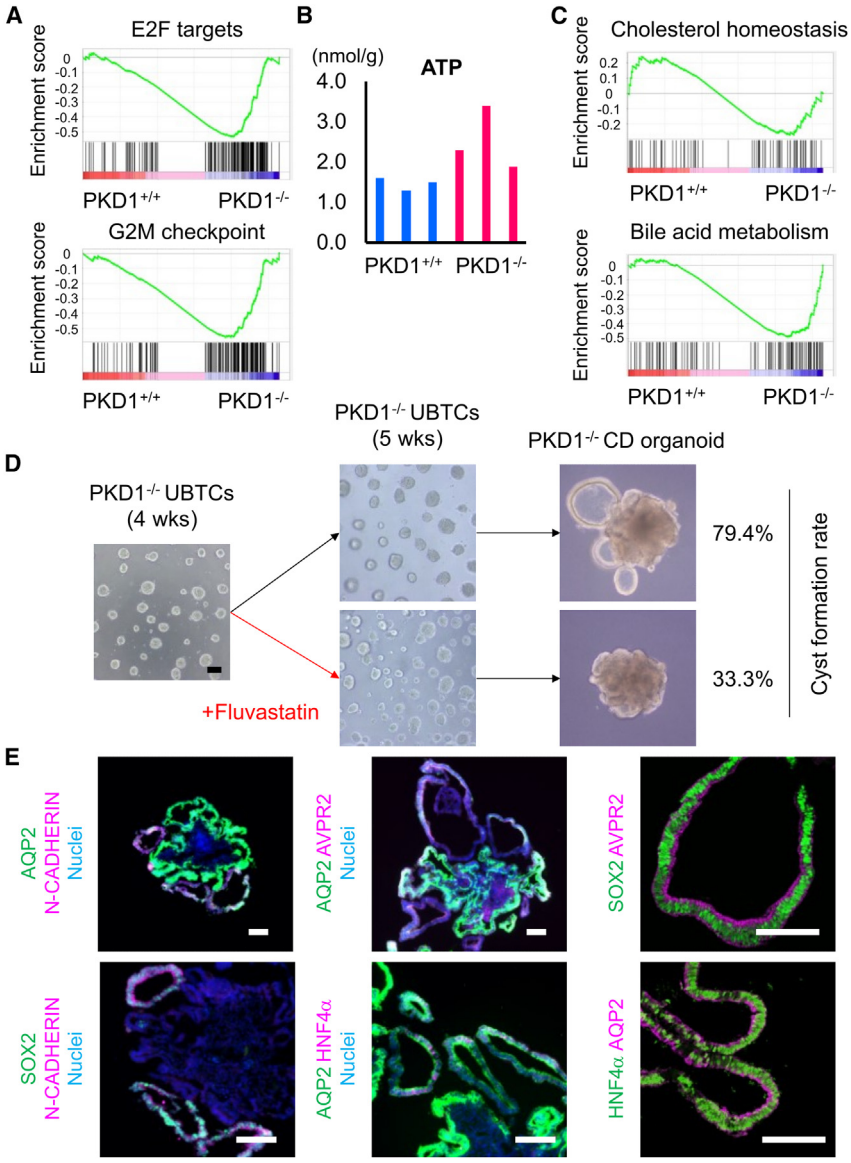

Figure 4. Identification of cystogenesis mechanisms and characterization of cyst cells

(A) GSEA enrichment plots for E2F targets and G2M checkpoint.

(B) Intracellular ATP levels in *PKD1*$^{+/+}$ and *PKD1*$^{-/-}$ UBTCs.

(C) GSEA enrichment plots for cholesterol homeostasis and bile acid metabolism.

(D) The cyst formation rates in CD organoids derived from *PKD1*$^{-/-}$ UBTCs that were treated with or without 1 μM fluvastatin were 33.3% (n = 27) and 79.4% (n = 34), respectively ($p < 0.05$ by chi-squared test).

(E) Immunostaining of day 21 CD organoids after 7 day CD maturation treatment of day 14 cyst-containing CD organoids reconstituted from 6-week-cultured UBTCs for AQP2 (green), N-CADHERIN (purple), and nuclei (blue; top left); for SOX2 (green), N-CADHERIN (purple), and nuclei (blue; bottom left); for AQP2 (green), AVPR2 (purple), and nuclei (blue; top middle); for AQP2 (green), HNF4α (purple), and nuclei (blue; bottom middle); for SOX2 (green) and AVPR2 (purple; top right); and for HNF4α (green) and AQP2 (purple; bottom right).

Scale bars, 100 μm in (D) and left and middle of (E) and 50 μm in right of (**E**). All data were obtained from *PKD1*$^{+/+}$ and *PKD1*$^{-/-}$ 1383D2-hiPSCs.

synthase inhibitor, venglustat (ibiglustat; 1 μM), tended to suppress cyst enlargement, although the effect was not statistically significant (Figure 5H). On the other hand, a potent Nrf2 activator, bardoxolone methyl (0.1 μM), and an EGFR inhibitor, tesevatinib (1 μM), both significantly suppressed cyst enlargement (Figure 5H). Moreover, fluvastatin suppressed cyst enlargement (Figure S9C) in addition to cyst formation (Figure 4D).

RAR agonists suppress cyst enlargement

In the process of establishing the HTS platform, we revealed that 0.1 μM of a potent RAR agonist, TTNPB, significantly suppresses cyst enlargement, although the suppression is weaker than that of a mTOR inhibitor, rapamycin (1 μM)[1] (Figures 6A, 6B, S9D, and S9E). Treatment with 0.1 μM ATRA also suppressed cyst enlargement, suggesting that the suppression by TTNPB is mediated through RAR signals (Figures 6A and S9D). TTNPB suppressed cyst cell proliferation without changing the apoptosis cell rate or AVPR2 expression (Figure S9F). To clarify the mechanisms of action of TTNPB, we performed a microarray analysis (Figure 6C). A GSEA showed that the "TGF-β signaling pathway," which is a crucial pathway for cyst enlargement and fibrosis,[39] was downregulated by TTNPB treatment (Figure 6D). Interestingly, "bile secretion," which includes *SLC2A1*, *CFTR*, and *HMGCR*, was also downregulated (Figures 6E and 6F). Since less glucose transport into cells via SLC2A1 and glycolysis limits cyst formation,[40] fluid secretion by CFTR causes cyst enlargement,[41] and HMG-CoA reductase inhibitors (i.e., statins) reduce cyst growth,[37,38] the downregulation of these genes indicates the suppression of cyst enlargement. Moreover, *MMP1*, which is highly secreted in the serum of patients with ADPKD,[42,43] was significantly reduced by TTNPB treatment (Figure 6F). The upregulated expression of cellular senescence markers is consistent with a previous report that showed that cellular senescence attenuates ADPKD progression (Figure 6G).[44] Then, focusing on the upregulation of *CDKN2B* expression by TTNPB treatment, we generated doxycycline-inducible CDKN2B-expressing hiPSCs. After the induction of cyst structures and the treatment with doxycycline, we found that the overexpression of CDKN2B attenuated cyst enlargement (Figures 6H and 6I), elucidating one mechanism by which RAR signals suppress cyst enlargement.

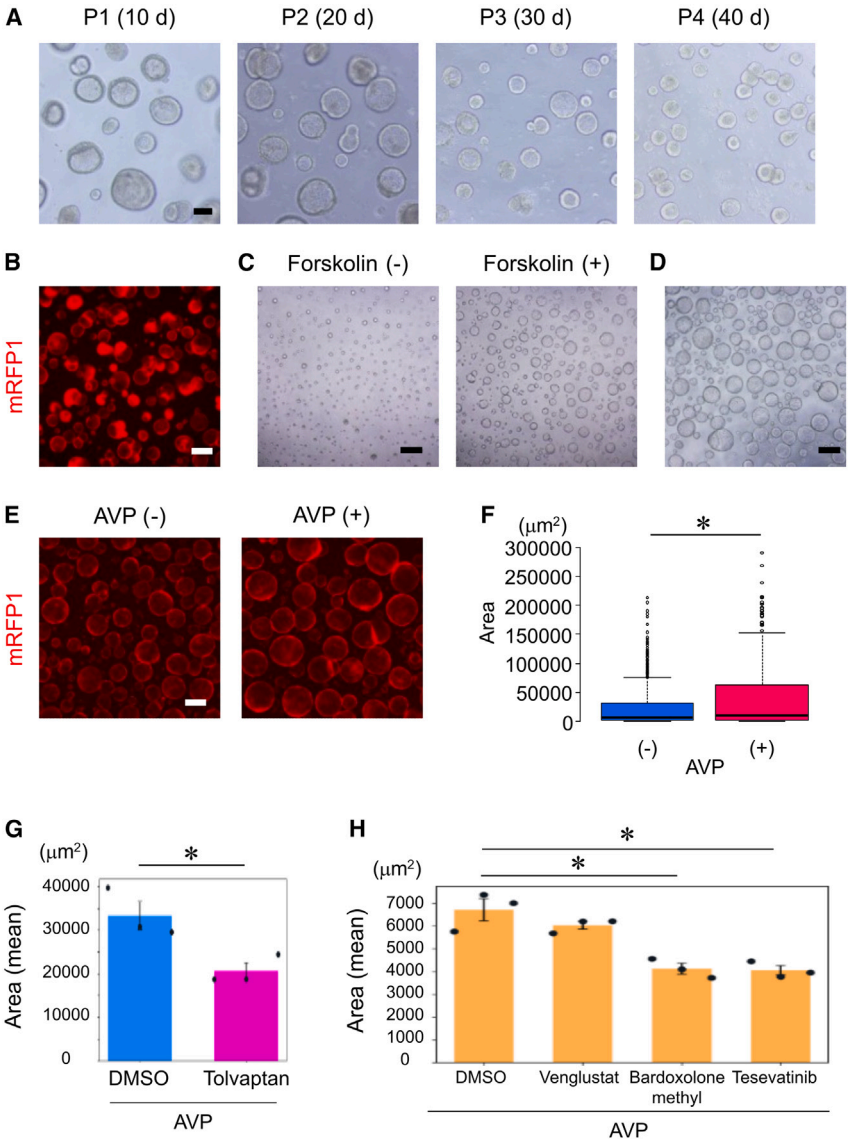

Figure 5. Development of an HTS platform for chemical compounds that suppress cyst enlargement

(A) Morphological changes of passaged cysts. Mechanically dissected cysts from CD organoids were passaged every 10 days.

(B) Morphology of two-times-passaged cysts. The mRFP1 expression monitors the insertion of gRNA vectors in the CRISPR-Cas9 piggyBac system.

(C) Morphology of single cyst cells cultured with or without 10 μM forskolin for 3 days.

(D) Morphology of cysts generated from the single cyst cells in (C) by an additional 2 days of culture after the removal of forskolin.

(E) Morphology of cysts treated with or without 2.5 μM arginine vassopressin (AVP) for 5 days.

(F) Cyst size after treatment with (n = 453) or without (n = 721) 2.5 μM AVP. *p < 0.001 by Mann-Whitney U test. Data are from three independent experiments and are presented as the mean ± SD.

(G) Cyst size after treatment with 2.5 μM AVP and 0.1% DMSO (n = 501) or 5 μM tolvaptan (n = 749). Data are from three independent experiments and are presented as the mean ± SD. *p < 0.05 by Student's t test.

(H) Cyst size after treatment with 2.5 μM AVP and 0.1% DMSO (n = 570), 1 μM venglustat (n = 518), 0.1 μM bardoxolone methyl (n = 528), or 1 μM tesevatinib (n = 522). Data are from three independent experiments and are presented as the mean ± SD. *p < 0.005 by one-way ANOVA with Tukey's test.

Scale bars, 100 μm in (A), (B), and (E) and 300 μm in (C) and (D). All data were obtained from *PKD1*$^{-/-}$ 1383D2-hiPSCs.

ATRA ameliorates ADPKD progression

Since ATRA has already been used as a therapeutic agent in patients with acute promyelocytic leukemia (APL),[15] we examined whether ATRA is effective in ADPKD model mice from the viewpoint of drug repurposing. To translate the *in vitro* results of ATRA on CD cyst enlargement *in vivo*, we used *Pkd1*$^{flox/flox}$: *Ksp-Cre* mice, in which *Pkd1* alleles are conditionally inactivated under kidney-specific *Ksp-Cre* recombinase expression in distal segments of the nephron and CDs.[45] These mice develop severe renal cystic disease with associated renal failure leading to death by around 2 weeks after birth. We intraperitoneally injected 5 or 10 mg/kg ATRA into postnatal day 3 (P3) mice and sacrificed the mice on P9 (Figure 7A). No significant body weight loss due to the ATRA treatment was observed (Figure 7B), but the two kidney-to-body weight (2KW/BW) ratio was significantly reduced in the ATRA-treated mouse groups compared with the vehicle-treated control mouse group (Figures 7C and 7D). Sagittal sections of the kidneys from the treated mice showed that cyst formation was suppressed in part of the kidney cortical parenchyma by 10 mg/kg ATRA treatment (Figure 7E). The cystic index, defined as the percentage of total cross-sectional area occupied by cysts, was reduced by 10 mg/kg ATRA treatment, although the decline was not statistically significant (Figure 7F). Blood urea nitrogen (BUN) levels were significantly lower in 10 mg/kg ATRA-treated mice compared with vehicle-treated control mice, indicating that renal functional decline was also suppressed by ATRA treatment (Figure 7G). These results suggest that ATRA treatment exerts therapeutic effects in both *in vitro* and *in vivo* ADPKD models.

DISCUSSION

To establish hPSC-based disease models, it is crucial to induce the cells into the affected cell types at the developmental stages when the target diseases develop. In mouse development, mutations of *Hnf1β*, an upstream regulator of renal-cyst-related genes, such as *Pkd2* and *Pkhd1*, induce cystogenesis in embryonic kidneys.[46] Therefore, we previously generated *HNF1β*$^{+/-}$ hiPSCs and induced UBOs, but we never observed cystogenesis,[10] suggesting insufficient differentiation of the UBOs. In

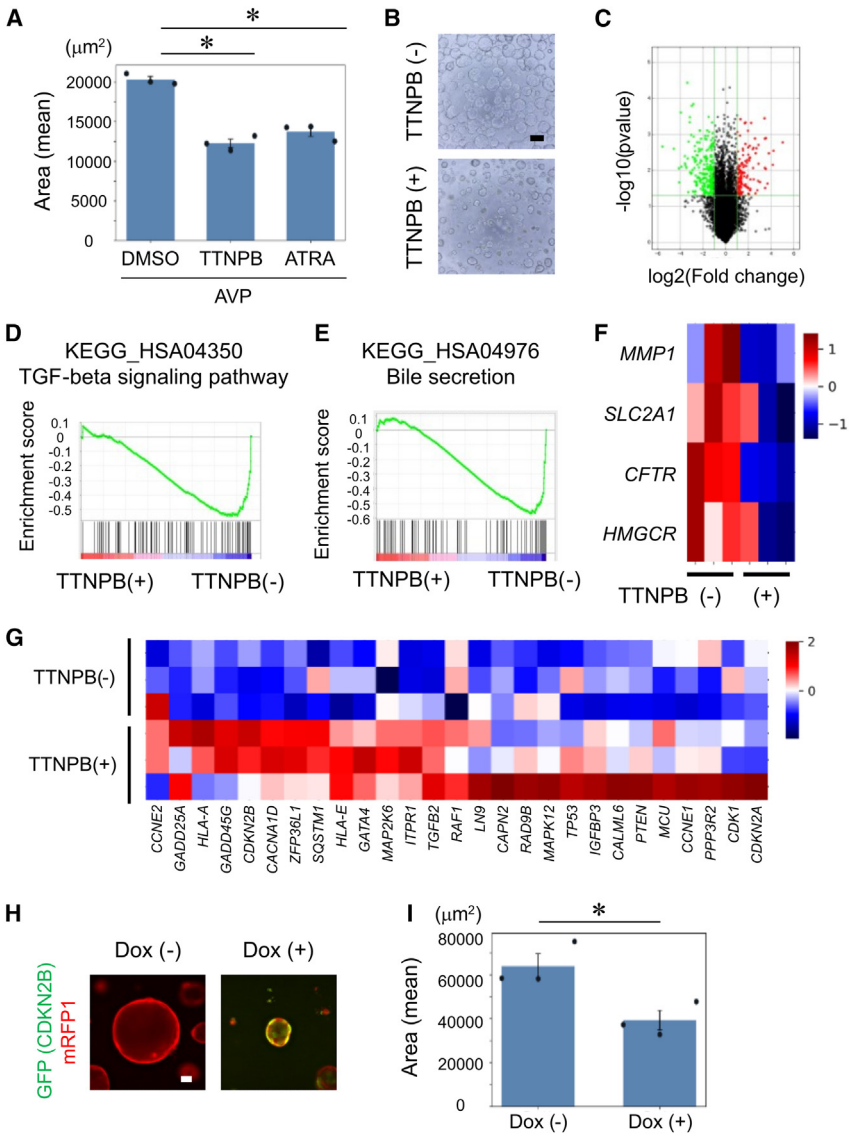

Figure 6. Suppression of cyst enlargement by RAR agonists

(A) Cyst size after treatment with 2.5 μM AVP and 0.1% DMSO (n = 455), 0.1 μM TTNPB (n = 664), or 0.1 μM ATRA (n = 803). Data are from three independent experiments and are presented as the mean ± SD. *p < 0.005 by one-way ANOVA with Tukey's test.

(B) Morphology of day 5 cysts cultured with or without 0.1 μM TTNPB.

(C) A volcano plot showing differentially expressed genes (DEGs) in cysts cultured with or without TTNPB evaluated by microarray.

(D and E) A GSEA enrichment plot for TGF-β signaling pathway (D) and bile secretion (E).

(F) A heatmap showing DEGs between cysts cultured with or without TTNPB evaluated by microarray.

(G) A heatmap showing that cellular senescence genes were upregulated by TTNPB treatment evaluated by microarray.

(H) Morphology of doxycycline-inducible CDKN2B-expressing CD cysts that were treated with (left) or without (right) 2 μM doxycycline. The GFP expression indicates CDKN2B expression, while the mRFP1 expression monitors the insertion of gRNA vectors in the CRISPR-Cas9 piggyBac system.

(I) Cyst size of doxycycline-inducible CDKN2B-expressing CD cysts after treatment with (n = 636) or without (n = 500) 2 μM doxycycline. Data are from three independent experiments and are presented as the mean ± SD. *p < 0.05 by Student's t test.

Scale bars, 300 μm in (B) and 50 μm in (H). All data were obtained from *PKD1*$^{-/-}$ 1383D2-hiPSCs.

addition, *AVPR2*, *AQP3*, and the CCD markers *COL4A5*, *PDE4D*, *TEX41*, and *GLIS3* were not expressed in CD cells differentiated from UBTCs without expansion culture.[10] On the other hand, a recent report showed that forskolin or vasopressin treatment induces cyst formation in UBOs differentiated from *PKD1*-mutant hiPSCs and ADPKD patient iPSCs, whereas non-treated UBOs do not form cysts.[9] These results suggest that previously reported hiPSC-derived UBOs are not sufficiently differentiated to initiate spontaneous cyst formation. In rodent ADPKD models, only homozygous mutations in *Pkd1* or *Pkd2* cause spontaneous cystogenesis during the late branching phases of UB. Although previous reports developed CD organoids from hPSCs, their characters resembled the early branching phase, as these organoids branched only a few times and contained only IMCD cells.[11,12]

Human UBs after the first 6–10 branches develop renal inner medullary tissues, such as the renal pelvis, papillae, and MCD cells, whereas the next 6–9 branches give rise to CCD cells.[47] In the current study, we established a long-term expansion culture method for UBTCs that advances their developmental stage into the late branching phase to generate cortical-cell-containing CD cells and recapitulates spontaneous cystogenesis when using *PKD1*$^{-/-}$ hiPSCs. However, the underlying mechanisms by which the long-term expansion culture advances the developmental stage remain to be elucidated. Assuming multiple UB branching events pattern preferably to CCD over MCD,[47] one possible explanation is that our long-term culture mimics this multiple branching. Another possibility is that a TGF-β inhibitor included in our long-term culture media may mimic the change in the surrounding stromal environment that results in the maturation of different segments of CD *in vivo*.[48] A third possibility is that multiple rounds of UBTC divisions shift the developmental potential of the cells without multiple branching events.

Whichever the mechanism, our method may become a powerful tool for the mass production of CD cysts. Indeed, approximately 2 × 10^{10} cyst structures can be generated from 4 × 10^{4} undifferentiated hiPSCs; thus, we can examine around 1 × 10^{8} different compound samples when using 200–300 cysts per compound (Figures S9B and S10). Although it has been reported

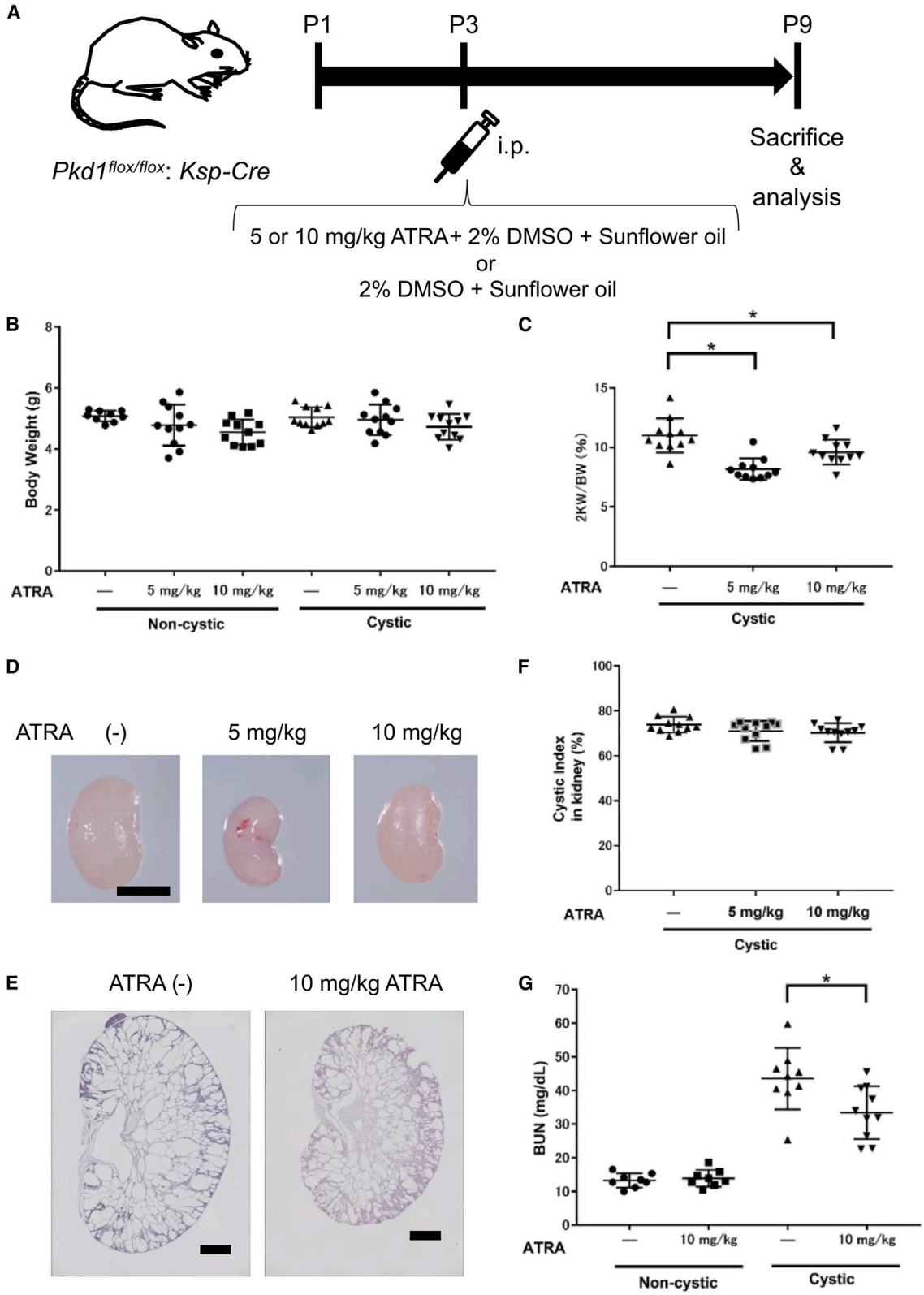

(legend on next page)

that spontaneous cystogenesis occurs by suspension culture of nephron organoids derived from *PKD1*- or *PKD2*-mutant human embryonic stem cells, not all those organoids formed cysts, which is unlike our current model, nor did tolvaptan suppress the nephron-organoid-derived cyst enlargement.[4–7]

It has been suggested that the pathogenesis of ADPKD can be divided into three phases: cyst initiation, cyst enlargement, and progression.[35] A recent report showed that pravastatin slows down cyst formation in children and young adults with ADPKD.[38] Substantial metabolic changes, including fatty acid metabolism, were reported to occur in children with ADPKD.[49] In our current study, by comparing UBTCs from *PKD1*$^{+/+}$ and *PKD1*$^{-/-}$ iPSCs, we showed that enhanced fatty acid oxidation and oxidative phosphorylation are triggers of cyst initiation, similar to ADPKD in mice,[35] and found that fluvastatin significantly suppresses cyst formation from *PKD1*$^{-/-}$ UBTCs. Therefore, our UBTC model may recapitulate phenotypes of the initiation stage of ADPKD. On the other hand, while it has been suggested that renal cyst formation occurs even during embryonic periods in patients with ADPKD[50] and a cynomolgus monkey ADPKD model,[51] adult CD-derived cysts grow slowly over decades in most patients with ADPKD. Moreover, aerobic glycolysis, rather than the TCA cycle and oxidative phosphorylation, was identified in the enlargement phase of ADPKD renal cysts.[35,52] In fact, previous clinical trials for ADPKD tested whether everolimus and sirolimus, which suppress aerobic glycolysis through the inhibition of mTOR signaling,[1] suppress cyst enlargement to give therapeutic effects. Although rapamycin, another inhibitor of mTOR signaling, suppressed cyst enlargement in our CD cyst model, it is still unclear whether our passaging culture for CD cyst cells and our HTS platform accurately reproduce the cyst enlargement phase in ADPKD. We created embryonic CD organoids to model metabolic changes along with ADPKD progression in our current study. Future studies should elucidate in detail the mechanisms of our CD cyst enlargement, including metabolic aspects, and also develop methods to generate adult CDs and model late-phase phenotypes of ADPKD using disease-specific iPSCs.

Although a recent report showed that the chemical compound quinazoline suppresses cyst formation in hPSC-derived nephron organoids, the efficacy of the compound in ADPKD model animals *in vivo* was not investigated.[7] On the other hand, we identified RAR agonists as crucial for suppressing cystogenesis, which may differ from known mechanisms that suppress the enlargement of CD cysts. Notably, therapeutic effects were shown in rapidly progressing ADPKD model mice. The upregulated expression of cellular senescence markers is suggested as one of the mechanisms by which RAR agonists suppress cyst enlargement in our current study. Although a previous study reported that ATRA alone does not suppress ADPKD cyst growth, the study used immortalized cyst cells, which may not accurately reflect the pathology of ADPKD due to the prevention of cell proliferation arrest with cellular senescence.[53] Future studies should examine whether RAR agonist treatments suppress cystogenesis and ameliorate kidney functional decline in late-stage ADPKD animal models.

Drug repurposing is a promising basis for drug discovery. Because existing drugs have known pharmacokinetics, pharmacodynamics, and safety profiles, new applications can go directly to phase 2 clinical trials. At the same time, disease models established from hPSCs reproduce pathological conditions, enabling more accurate confirmation of the therapeutic effects and therefore improving the success rate of drug repurposing. Consistently, several groups have identified drug-repurposing candidates using hPSC-derived disease models,[54] suggesting the promise of ATRA in our model for the establishment of new ADPKD treatment.

In conclusion, by advancing the developmental stage of UBTCs by an expansion culture, we successfully established a spontaneous and efficient CD cystogenesis model *in vitro*. Moreover, we reduced cystogenesis by using statin and identified RAR agonists as effective chemical compounds to suppress cyst enlargement. We also confirmed that ATRA ameliorates disease progression *in vivo* in ADPKD model mice. Therefore, the present study demonstrates the usefulness of kidney organoid technology in drug discovery for ADPKD.

Limitations of the study

By advancing the developmental stages of UBTCs with long-term expansion culture, we successfully generated cortical-cell-containing CD organoids that are applicable to model ADPKD cystogenesis. However, UBTCs cultured for 2 or 6 weeks are equally capable of differentiating into CD organoids that express AQP2, but 2-week-cultured UBTCs generated slightly less CCDs than 6-week-cultured UBTCs. In addition, ATP6V1B1^{+} ICs were generated from 3-week-cultured UBTCs

Figure 7. Treatment of ADPKD model mice with ATRA

(A) A schematic illustration of the treatment of ADPKD model mice with ATRA. i.p., intraperitoneal injection.

(B) Body weight of mice with or without ATRA administration. The data are presented as the mean ± SD (n = 9 in non-cystic with vehicle treatment and n = 11 in the other conditions). Not significant by one-way ANOVA with Tukey's test.

(C) The ratio of two kidney weight (2KW) to body weight (BW). The data are presented as the mean ± SD (n = 11). *p < 0.05 by one-way ANOVA with Tukey's test.

(D) The gross appearance of freshly collected whole kidneys from P9 *Pkd1*$^{flox/flox}$:*Ksp-Cre* mice treated with vehicle (DMSO and sunflower oil; left), 5 mg/kg ATRA (middle), and 10 mg/kg ATRA (right).

(E) Section images of cystic kidneys from P9 *Pkd1*$^{flox/flox}$:*Ksp-Cre* mice treated with or without 10 mg/kg ATRA.

(F) The cystic index, which indicates the severity of PKD, in P9 *Pkd1*$^{flox/flox}$:*Ksp-Cre* mice after treatment with vehicle or 5 and 10 mg/kg ATRA. The data are presented as the mean ± SD (n = 11). Note that although there are no significant differences using one-way ANOVA with Tukey's test, there is a statistically significant difference between the 10 mg/kg ATRA and vehicle groups using a two-tailed Student's t test (p < 0.05).

(G) BUN levels in P9 *Pkd1*$^{flox/flox}$:*Ksp-Cre* mice treated with or without 10 mg/kg ATRA. The data are presented as the mean ± SD (n = 8 in non-cystic, n = 9 in cystic with vehicle treatment, and n = 10 in cystic with ATRA treatment). *p < 0.005 by one-way ANOVA with Tukey's test. Non-cystic, *Pkd1*$^{flox/-}$ mice; Cystic, *Pkd1*$^{flox/flox}$:*Ksp-Cre* mice.

Scale bars, 5 mm in (D) and 1 mm in (E).

but not from 6-week-cultured UBTCs. Therefore, future efforts in this field are warranted to clarify the detailed mechanisms underlying the UBTC proliferation by A83-01 and the developmental advancement of UBTCs by the long-term expansion culture. Although the effectiveness of our strategy to induce cortical-cell-containing CD organoids was confirmed in this study, an efficient induction method for CCDs has not been established, and the underlying developmental mechanisms of different CD components remain controversial. The establishment of benchmarks for different CD cell types by performing functional evaluations and elucidating detailed gene expression profiles may contribute to the further development of kidney regeneration from hPSCs. Further understanding of the structural changes of CD epithelia associated with cystogenesis and the cystogenesis mechanisms are also required since *PKD1*$^{-/-}$ UBTCs form cysts without CD induction. The detailed mechanisms for the suppression of cystogenesis by RAR agonists also require more research. Finally, HTS using the established platform should be conducted to identify other therapeutic drug candidates.

STAR★METHODS

Detailed methods are provided in the online version of this paper and include the following:

- KEY RESOURCES TABLE
- RESOURCE AVAILABILITY
  - Lead contact
  - Materials availability
  - Data and code availability
- EXPERIMENTAL MODEL AND STUDY PARTICIPANT DETAILS
  - Animals
  - Cell lines
- METHOD DETAILS
  - Directed differentiation
  - Generation of PKD1$^{-/-}$ hiPSCs
  - Cyst enlargement and inhibition of cyst formation
  - Expansion of cyst cells
  - HTS platform
  - Overexpression of CDKN2B in cyst cells
  - RT-PCR and quantitative RT-PCR
  - Flow cytometry analysis
  - Bulk RNA sequencing analysis
  - Single cell RNA-sequencing
  - Microarray analysis
  - Metabolome analysis
  - ATRA treatment
  - Blood sample measurements
  - Histology and cystic index determination
  - Immunostaining
- QUANTIFICATION AND STATISTICAL ANALYSIS

SUPPLEMENTAL INFORMATION

Supplemental information can be found online at https://doi.org/10.1016/j.celrep.2023.113431.

ACKNOWLEDGMENTS

We thank Drs. Keisuke Okita and Tatsuya Shimizu, CiRA, Kyoto University, for kindly providing the cell lines; Drs. Akitsu Hotta and Knut Woltjen, CiRA, Kyoto University, for kindly providing the piggyBac vectors; Dr. Peter Karagiannis for critically reading and revising the manuscript; and Drs. Ayano Ueno and Maki Ohishi, Institute for Advanced Bioscience, Keio University, DNAFORM Co., Ltd., and Filgen Co., Ltd., for technical support. This study was partially supported by Otsuka Pharmaceutical Co., Ltd.; by the Japan Society for the Promotion of Science (JSPS) through its Grant-in-Aid for Scientific Research (C) (JSPS KAKENHI grant number 19K08703) to S.-I.M. and CREST (grant number JPMJCR2123) to T.S.; by the Japan Agency for Medical Research and Development (AMED) through its research grant "The Program for Technological Innovation of Regenerative Medicine (JP23bm0704072)" to S.-I.M., "Core Center for iPS Cell Research (JP22bm0104001) and The Acceleration Program for Intractable Diseases Research utilizing Disease-specific iPS cells (JP22bm0804013), Research Center Network for Realization of Regenerative Medicine and R&D Program of Regenerative Medicine and Cell and Gene Therapy from the Basic to Nonclinical Phase, Acceleration Program of R&D and implementation for Regenerative Medicine and Cell and Gene Therapy (JP23bm1123002)" to K.O., and "Moonshot Research and Development Program (JP21zf0127001)" to T.S.; and by the iPS Cell Research Fund.

AUTHOR CONTRIBUTIONS

S.-I.M., S.N., and K.O. designed this study. S.-I.M., F.H., H.M., A.N., N.K., H.O., K.T., Y.N., A.K., S.Y., K.M., and M.R. performed the experiments. S.-I.M., A.W., T.S., S.N., and K.O. analyzed the data. K.O. supervised the study. S.-I.M. and K.O. drafted the manuscript. All authors discussed the results and commented on the manuscript.

DECLARATION OF INTERESTS

S.-I.M. is a scientific advisor of Rege Nephro Co., Ltd. K.O. is a founder and member of the scientific advisory boards of iPS Portal, Inc., and a founder and chief scientific advisor of Rege Nephro Co., Ltd. S.-I.M., M.R., and K.O. are the inventors of Japanese patent no. 7162349.

Received: October 17, 2022
Revised: December 15, 2022
Accepted: October 30, 2023
Published: November 30, 2023

REFERENCES

1. Cornec-Le Gall, E., Alam, A., and Perrone, R.D. (2019). Autosomal dominant polycystic kidney disease. Lancet *393*, 919–935. https://doi.org/10.1016/S0140-6736(18)32782-X.
2. Bergmann, C., Guay-Woodford, L.M., Harris, P.C., Horie, S., Peters, D.J.M., and Torres, V.E. (2018). Polycystic kidney disease. Nat. Rev. Dis. Primers *4*, 50. https://doi.org/10.1038/s41572-018-0047-y.
3. Devuyst, O., Burrow, C.R., Smith, B.L., Agre, P., Knepper, M.A., and Wilson, P.D. (1996). Expression of aquaporins-1 and -2 during nephrogenesis and in autosomal dominant polycystic kidney disease. Am. J. Physiol. *271*, F169–F183. https://doi.org/10.1152/ajprenal.1996.271.1.F169.
4. Freedman, B.S., Brooks, C.R., Lam, A.Q., Fu, H., Morizane, R., Agrawal, V., Saad, A.F., Li, M.K., Hughes, M.R., Werff, R.V., et al. (2015). Modelling kidney disease with CRISPR-mutant kidney organoids derived from human pluripotent epiblast spheroids. Nat. Commun. *6*, 8715. https://doi.org/10.1038/ncomms9715.
5. Cruz, N.M., Song, X., Czerniecki, S.M., Gulieva, R.E., Churchill, A.J., Kim, Y.K., Winston, K., Tran, L.M., Diaz, M.A., Fu, H., et al. (2017). Organoid cystogenesis reveals a critical role of microenvironment in human polycystic kidney disease. Nat. Mater. *16*, 1112–1119. https://doi.org/10.1038/nmat4994.

6. Czerniecki, S.M., Cruz, N.M., Harder, J.L., Menon, R., Annis, J., Otto, E.A., Gulieva, R.E., Islas, L.V., Kim, Y.K., Tran, L.M., et al. (2018). High-Throughput Screening Enhances Kidney Organoid Differentiation from Human Pluripotent Stem Cells and Enables Automated Multidimensional Phenotyping. Cell Stem Cell *22*, 929–940.e4. https://doi.org/10.1016/j.stem.2018.04.022.

7. Tran, T., Song, C.J., Nguyen, T., Cheng, S.Y., McMahon, J.A., Yang, R., Guo, Q., Der, B., Lindström, N.O., Lin, D.C.H., and McMahon, A.P. (2022). A scalable organoid model of human autosomal dominant polycystic kidney disease for disease mechanism and drug discovery. Cell Stem Cell *29*, 1083–1101.e7. https://doi.org/10.1016/j.stem.2022.06.005.

8. Shimizu, T., Mae, S.I., Araoka, T., Okita, K., Hotta, A., Yamagata, K., and Osafune, K. (2020). A novel ADPKD model using kidney organoids derived from disease-specific human iPSCs. Biochem. Biophys. Res. Commun. *529*, 1186–1194. https://doi.org/10.1016/j.bbrc.2020.06.141.

9. Kuraoka, S., Tanigawa, S., Taguchi, A., Hotta, A., Nakazato, H., Osafune, K., Kobayashi, A., and Nishinakamura, R. (2020). PKD1-Dependent Renal Cystogenesis in Human Induced Pluripotent Stem Cell-Derived Ureteric Bud/Collecting Duct Organoids. J. Am. Soc. Nephrol. *31*, 2355–2371. https://doi.org/10.1681/ASN.2020030378.

10. Mae, S.I., Ryosaka, M., Sakamoto, S., Matsuse, K., Nozaki, A., Igami, M., Kabai, R., Watanabe, A., and Osafune, K. (2020). Expansion of Human iPSC-Derived Ureteric Bud Organoids with Repeated Branching Potential. Cell Rep. *32*, 107963. https://doi.org/10.1016/j.celrep.2020.107963.

11. Zeng, Z., Huang, B., Parvez, R.K., Li, Y., Chen, J., Vonk, A.C., Thornton, M.E., Patel, T., Rutledge, E.A., Kim, A.D., et al. (2021). Generation of patterned kidney organoids that recapitulate the adult kidney collecting duct system from expandable ureteric bud progenitors. Nat. Commun. *12*, 3641. https://doi.org/10.1038/s41467-021-23911-5.

12. Shi, M., McCracken, K.W., Patel, A.B., Zhang, W., Ester, L., Valerius, M.T., and Bonventre, J.V. (2022). Human ureteric bud organoids recapitulate branching morphogenesis and differentiate into functional collecting duct cell types. Nat. Biotechnol. *41*, 252–261. https://doi.org/10.1038/s41587-022-01429-5.

13. Clevers, H. (2016). Modeling Development and Disease with Organoids. Cell *165*, 1586–1597. https://doi.org/10.1016/j.cell.2016.05.082.

14. Shakya, R., Jho, E.H., Kotka, P., Wu, Z., Kholodilov, N., Burke, R., D'Agati, V., and Costantini, F. (2005). The role of GDNF in patterning the excretory system. Dev. Biol. *283*, 70–84. https://doi.org/10.1016/j.ydbio.2005.04.008.

15. Ohno, R., Yoshida, H., Fukutani, H., Naoe, T., Ohshima, T., Kyo, T., Endoh, N., Fujimoto, T., Kobayashi, T., Hiraoka, A., et al. (1993). Multi-institutional Study of All-Trans-Retinoic Acid as a Differentiation Therapy of Refractory Acute Promyelocytic Leukemia. Leukemia *7*, 1722–1727.

16. Nakagawa, M., Taniguchi, Y., Senda, S., Takizawa, N., Ichisaka, T., Asano, K., Morizane, A., Doi, D., Takahashi, J., Nishizawa, M., et al. (2014). A novel efficient feeder-free culture system for the derivation of human induced pluripotent stem cells. Sci. Rep. *4*, 3594. https://doi.org/10.1038/srep03594.

17. Plisov, S.Y., Yoshino, K., Dove, L.F., Higinbotham, K.G., Rubin, J.S., and Perantoni, A.O. (2001). TGF beta 2, LIF and FGF2 cooperate to induce nephrogenesis. Development *128*, 1045–1057.

18. Bush, K.T., Sakurai, H., Steer, D.L., Leonard, M.O., Sampogna, R.V., Meyer, T.N., Schwesinger, C., Qiao, J., and Nigam, S.K. (2004). TGF-beta superfamily members modulate growth, branching, shaping, and patterning of the ureteric bud. Dev. Biol. *266*, 285–298. https://doi.org/10.1016/j.ydbio.2003.10.023.

19. Takayama, M., Miyatake, K., and Nishida, E. (2014). Identification and characterization of retinoic acid-responsive genes in mouse kidney development. Gene Cell. *19*, 637–649. https://doi.org/10.1111/gtc.12163.

20. Toyoda, D., Taguchi, A., Chiga, M., Ohmori, T., and Nishinakamura, R. (2013). Sall4 Is Transiently Expressed in the Caudal Wolffian Duct and the Ureteric Bud, but Dispensable for Kidney Development. PLoS One *8*, e68508. https://doi.org/10.1371/journal.pone.0068508.

21. Schmidt-Ott, K.M., Chen, X., Paragas, N., Levinson, R.S., Mendelsohn, C.L., and Barasch, J. (2006). c-kit delineates a distinct domain of progenitors in the developing kidney. Dev. Biol. *299*, 238–249. https://doi.org/10.1016/j.ydbio.2006.07.026.

22. Rutledge, E.A., Benazet, J.D., and McMahon, A.P. (2017). Cellular heterogeneity in the ureteric progenitor niche and distinct profiles of branching morphogenesis in organ development. Development *144*, 3177–3188. https://doi.org/10.1242/dev.149112.

23. Naganuma, H., Miike, K., Ohmori, T., Tanigawa, S., Ichikawa, T., Yamane, M., Eto, M., Niwa, H., Kobayashi, A., and Nishinakamura, R. (2021). Molecular detection of maturation stages in the developing kidney. Dev. Biol. *470*, 62–73. https://doi.org/10.1016/j.ydbio.2020.11.002.

24. Paramos-de-Carvalho, D., Jacinto, A., and Saúde, L. (2021). The right time for senescence. Elife *10*, e72449. https://doi.org/10.7554/eLife.72449.

25. Hao, Y., Hao, S., Andersen-Nissen, E., Mauck, W.M., Zheng, S., Butler, A., Lee, M.J., Wilk, A.J., Darby, C., Zager, M., et al. (2021). Integrated analysis of multimodal single-cell data. Cell *184*, 3573–3587.e29. https://doi.org/10.1016/j.cell.2021.04.048.

26. Lake, B.B., Chen, S., Hoshi, M., Plongthongkum, N., Salamon, D., Knoten, A., Vijayan, A., Venkatesh, R., Kim, E.H., Gao, D., et al. (2019). A single-nucleus RNA-sequencing pipeline to decipher the molecular anatomy and pathophysiology of human kidneys. Nat. Commun. *10*, 2832. https://doi.org/10.1038/s41467-019-10861-2.

27. Wang, G., Heijs, B., Kostidis, S., Rietjens, R.G.J., Koning, M., Yuan, L., Tiemeier, G.L., Mahfouz, A., Dumas, S.J., Giera, M., et al. (2022). Spatial dynamic metabolomics identifies metabolic cell fate trajectories in human kidney differentiation. Cell Stem Cell *29*, 1580–1593.e7. https://doi.org/10.1016/j.stem.2022.10.008.

28. Tian, Z., and Liang, M. (2021). Renal metabolism and hypertension. Nat. Commun. *12*, 963. https://doi.org/10.1038/s41467-021-21301-5.

29. Lu, W., Peissel, B., Babakhanlou, H., Pavlova, A., Geng, L., Fan, X., Larson, C., Brent, G., and Zhou, J. (1997). Perinatal lethality with kidney and pancreas defects in mice with a targetted Pkd1 mutation. Nat. Genet. *17*, 179–181. https://doi.org/10.1038/ng1097-179.

30. Okita, K., Yamakawa, T., Matsumura, Y., Sato, Y., Amano, N., Watanabe, A., Goshima, N., and Yamanaka, S. (2013). An efficient nonviral method to generate integration-free human-induced pluripotent stem cells from cord blood and peripheral blood cells. Stem Cell. *31*, 458–466. https://doi.org/10.1002/stem.1293.

31. Ishida, K., Xu, H., Sasakawa, N., Lung, M.S.Y., Kudryashev, J.A., Gee, P., and Hotta, A. (2018). Site-specific randomization of the endogenous genome by a regulatable CRISPR-Cas9 piggyBac system in human cells. Sci. Rep. *8*, 310. https://doi.org/10.1038/s41598-017-18568-4.

32. Roitbak, T., Ward, C.J., Harris, P.C., Bacallao, R., Ness, S.A., and Wandinger-Ness, A. (2004). A polycystin-1 multiprotein complex is disrupted in polycystic kidney disease cells. Mol. Biol. Cell *15*, 1334–1346. https://doi.org/10.1091/mbc.e03-05-0296.

33. Rahimmanesh, I., and Fatehi, R. (2020). Systems biology approaches toward autosomal dominant polycystic kidney disease (ADPKD). Clin. Transl. Med. *9*, 1. https://doi.org/10.1186/s40169-019-0254-5.

34. Allen, E., Piontek, K.B., Garrett-Mayer, E., Garcia-Gonzalez, M., Gorelick, K.L., and Germino, G.G. (2006). Loss of polycystin-1 or polycystin-2 results in dysregulated apolipoprotein expression in murine tissues via alterations in nuclear hormone receptors. Hum. Mol. Genet. *15*, 11–21. https://doi.org/10.1093/hmg/ddi421.

35. Malas, T.B., Leonhard, W.N., Bange, H., Granchi, Z., Hettne, K.M., Van Westen, G.J.P., Price, L.S., t Hoen, P.A.C., and Peters, D.J.M. (2020). Prioritization of novel ADPKD drug candidates from disease-stage specific gene expression profiles. EBioMedicine *51*, 102585. https://doi.org/10.1016/j.ebiom.2019.11.046.

36. Grundy, S.M. (1988). HMG-CoA reductase inhibitors for treatment of hypercholesterolemia. N. Engl. J. Med. *319*, 24–33. https://doi.org/10.1056/NEJM198807073190105.

37. Zafar, I., Tao, Y., Falk, S., McFann, K., Schrier, R.W., and Edelstein, C.L. (2007). Effect of statin and angiotensin-converting enzyme inhibition on structural and hemodynamic alterations in autosomal dominant polycystic kidney disease model. Am. J. Physiol. Renal Physiol. *293*, F854–F859. https://doi.org/10.1152/ajprenal.00059.2007.

38. Cadnapaphornchai, M.A., George, D.M., McFann, K., Wang, W., Gitomer, B., Strain, J.D., and Schrier, R.W. (2014). Effect of pravastatin on total kidney volume, left ventricular mass index, and microalbuminuria in pediatric autosomal dominant polycystic kidney disease. Clin. J. Am. Soc. Nephrol. *9*, 889–896. https://doi.org/10.2215/CJN.08350813.

39. Zhang, Y., Dai, Y., Raman, A., Daniel, E., Metcalf, J., Reif, G., Pierucci-Alves, F., and Wallace, D.P. (2020). Overexpression of TGF-beta1 induces renal fibrosis and accelerates the decline in kidney function in polycystic kidney disease. Am. J. Physiol. Renal Physiol. *319*, F1135–F1148. https://doi.org/10.1152/ajprenal.00366.2020.

40. Rowe, I., Chiaravalli, M., Mannella, V., Ulisse, V., Quilici, G., Pema, M., Song, X.W., Xu, H., Mari, S., Qian, F., et al. (2013). Defective glucose metabolism in polycystic kidney disease identifies a new therapeutic strategy. Nat. Med. *19*, 488–493. https://doi.org/10.1038/nm.3092.

41. Hanaoka, K., and Guggino, W.B. (2000). cAMP regulates cell proliferation and cyst formation in autosomal polycystic kidney disease cells. J. Am. Soc. Nephrol. *11*, 1179–1187. https://doi.org/10.1681/ASN.V1171179.

42. Nakamura, T., Ushiyama, C., Suzuki, S., Ebihara, I., Shimada, N., and Koide, H. (2000). Elevation of serum levels of metalloproteinase-1, tissue inhibitor of metalloproteinase-1 and type IV collagen, and plasma levels of metalloproteinase-9 in polycystic kidney disease. Am. J. Nephrol. *20*, 32–36. https://doi.org/10.1159/000013552.

43. Ameku, T., Taura, D., Sone, M., Numata, T., Nakamura, M., Shiota, F., Toyoda, T., Matsui, S., Araoka, T., Yasuno, T., et al. (2016). Identification of MMP1 as a novel risk factor for intracranial aneurysms in ADPKD using iPSC models. Sci. Rep. *6*, 30013. https://doi.org/10.1038/srep30013.

44. Park, J.Y., Schutzer, W.E., Lindsley, J.N., Bagby, S.P., Oyama, T.T., Anderson, S., and Weiss, R.H. (2007). p21 is decreased in polycystic kidney disease and leads to increased epithelial cell cycle progression: roscovitine augments p21 levels. BMC Nephrol. *8*, 12. https://doi.org/10.1186/1471-2369-8-12.

45. Shibazaki, S., Yu, Z., Nishio, S., Tian, X., Thomson, R.B., Mitobe, M., Louvi, A., Velazquez, H., Ishibe, S., Cantley, L.G., et al. (2008). Cyst formation and activation of the extracellular regulated kinase pathway after kidney specific inactivation of Pkd1. Hum. Mol. Genet. *17*, 1505–1516. https://doi.org/10.1093/hmg/ddn039.

46. Gresh, L., Fischer, E., Reimann, A., Tanguy, M., Garbay, S., Shao, X., Hiesberger, T., Fiette, L., Igarashi, P., Yaniv, M., and Pontoglio, M. (2004). A transcriptional network in polycystic kidney disease. EMBO J. *23*, 1657–1668. https://doi.org/10.1038/sj.emboj.7600160.

47. Ishiyama, H., Ishikawa, A., Kitazawa, H., Fujii, S., Matsubayashi, J., Yamada, S., and Takakuwa, T. (2018). Branching morphogenesis of the urinary collecting system in the human embryonic metanephros. PLoS One *13*, e0203623. https://doi.org/10.1371/journal.pone.0203623.

48. Wilson, S.B., Howden, S.E., Vanslambrouck, J.M., Dorison, A., Alquicira-Hernandez, J., Powell, J.E., and Little, M.H. (2022). DevKidCC allows for robust classification and direct comparisons of kidney organoid datasets. Genome Med. *14*, 19. https://doi.org/10.1186/s13073-022-01023-z.

49. Baliga, M.M., Klawitter, J., Christians, U., Hopp, K., Chonchol, M., Gitomer, B.Y., Cadnapaphornchai, M.A., and Klawitter, J. (2021). Metabolic profiling in children and young adults with autosomal dominant polycystic kidney disease. Sci. Rep. *11*, 6629. https://doi.org/10.1038/s41598-021-84609-8.

50. Grantham, J.J., Cook, L.T., Wetzel, L.H., Cadnapaphornchai, M.A., and Bae, K.T. (2010). Evidence of extraordinary growth in the progressive enlargement of renal cysts. Clin. J. Am. Soc. Nephrol. *5*, 889–896. https://doi.org/10.2215/CJN.00550110.

51. Tsukiyama, T., Kobayashi, K., Nakaya, M., Iwatani, C., Seita, Y., Tsuchiya, H., Matsushita, J., Kitajima, K., Kawamoto, I., Nakagawa, T., et al. (2019). Monkeys mutant for PKD1 recapitulate human autosomal dominant polycystic kidney disease. Nat. Commun. *10*, 5517. https://doi.org/10.1038/s41467-019-13398-6.

52. Nowak, K.L., and Hopp, K. (2020). Metabolic Reprogramming in Autosomal Dominant Polycystic Kidney Disease: Evidence and Therapeutic Potential. Clin. J. Am. Soc. Nephrol. *15*, 577–584. https://doi.org/10.2215/CJN.13291019.

53. Nguyen, Q.T.T., Hoang, T.X., Ryu, H., Oh, K.H., and Kim, J.Y. (2021). Synergistic Antiproliferative Effects of All-Trans Retinoic Acid and Paclitaxel on Autosomal Dominant Polycystic Kidney Disease Epithelial Cells. BioMed Res. Int. *2021*, 1242916. https://doi.org/10.1155/2021/1242916.

54. Tsujimoto, H., and Osafune, K. (2022). Current status and future directions of clinical applications using iPS cells-focus on Japan. FEBS J. *289*, 7274–7291. https://doi.org/10.1111/febs.16162.

55. Kim, S.I., Oceguera-Yanez, F., Sakurai, C., Nakagawa, M., Yamanaka, S., and Woltjen, K. (2016). Inducible Transgene Expression in Human iPS Cells Using Versatile All-in-One piggyBac Transposons. Methods Mol Biol *1357*, 111–131. https://doi.org/10.1007/7651_2015_251.

56. Kanda, Y. (2013). Investigation of the freely available easy-to-use software 'EZR' for medical statistics. Bone Marrow Transplant. *48*, 452–458. https://doi.org/10.1038/bmt.2012.244.

57. Sugimoto, M., Wong, D.T., Hirayama, A., Soga, T., and Tomita, M. (2010). Capillary electrophoresis mass spectrometry-based saliva metabolomics identified oral, breast and pancreatic cancer-specific profiles. Metabolomics *6*, 78–95. https://doi.org/10.1007/s11306-009-0178-y.

58. Qiu, X., Hill, A., Packer, J., Lin, D., Ma, Y.A., and Trapnell, C. (2017). Single-cell mRNA quantification and differential analysis with Census. Nat. Methods. *14*, 309–315. https://doi.org/10.1038/nmeth.4150.

59. Stuart, T., Butler, A., Hoffman, P., Hafemeister, C., Papalexi, E., Mauck, W.M., 3rd, Hao, Y., Stoeckius, M., Smibert, P., and Satija, R. (2019). Comprehensive Integration of Single-Cell Data. Cell *177*, 1888–1902.e21. https://doi.org/10.1016/j.cell.2019.05.031.

60. Ryosaka, M., Mae, S.I., and Osafune, K. (2022). Protocol for the generation and expansion of human iPS cell-derived ureteric bud organoids. STAR Protoc. *3*, 101484. https://doi.org/10.1016/j.xpro.2022.101484.

61. Soga, T., Baran, R., Suematsu, M., Ueno, Y., Ikeda, S., Sakurakawa, T., Kakazu, Y., Ishikawa, T., Robert, M., Nishioka, T., and Tomita, M. (2006). Differential metabolomics reveals ophthalmic acid as an oxidative stress biomarker indicating hepatic glutathione consumption. J. Biol. Chem. *281*, 16768–16776. https://doi.org/10.1074/jbc.M601876200.

62. Soga, T., Igarashi, K., Ito, C., Mizobuchi, K., Zimmermann, H.P., and Tomita, M. (2009). Metabolomic profiling of anionic metabolites by capillary electrophoresis mass spectrometry. Anal. Chem. *81*, 6165–6174. https://doi.org/10.1021/ac900675k.

STAR★METHODS

KEY RESOURCES TABLE

REAGENT or RESOURCE	SOURCE	IDENTIFIER
Antibodies		
Rabbit anti-AQP2	Sigma Aldrich	Cat# A7310; RRID: AB_476762
Mouse anti-AQP2	Santa Cruz	Cat#sc-515770; RRID: AB_2810957
Rabbit anti-ARL13B	Proteintech	Cat# 17711-1-AP; RRID: AB_2060867
Mouse anti-ATP6V1B1	Santa Cruz	Cat# sc-55544; RRID: AB_831844
Rabbit anti-ATP6V1B1	Sigma Aldrich	Cat#HPA031847
Biotin anti-AVPR2	LifeSpan BioSciences	Cat# LS-A103135-100
Rabbit anti-AVPR2	Millipore	Cat# AB1797P; RRID: AB_11214157
Rabbit anti-CK19	Abcam	Cat# ab52625; RRID: AB_2281020
Rabbit ant-Cleaved Caspase-3	Cell signaling	Cat#9661S RRID: AB_2341188
Mouse anti-EZRIN	Abcam	Cat#Ab4069; RRID: AB_304261
Rabbit anti-GATA3	Cell signaling	Cat#5852S; RRID: AB_10835690
Goat anti-GATA3	R&D	Cat#AF2605; RRID: AB_2108571
Mouse anti-HNF4α	Invitrogen	Cat# MA1-199; RRID: AB_2633309
Biotin Mouse anti-IgG2a, κ Isotype Control	BioLegend	Cat#400203
Mouse anti-Ki67	BD	Cat# 556003; RRID: AB_396287
Mouse anti-N-CADHERIN	BD	Cat# 610920; RRID: AB_2077527
Rabbit anti-PAX2	BioLegend	Cat#PRB-276P; RRID: AB_291611
Goat anti-PAX2	R&D	Cat#AF3364; RRID: AB_10889828
Biotin Mouse anti-PCNA	BioLegend	Cat#307904 RRID: AB_314694
Goat anti-RET	R&D	Cat#AF1485 RRID: AB_354820
Rabbit anti-SOX2	Cell signaling	Cat#3579S; RRID: AB_2195767
Donkey anti-Mouse IgG- Alexa Fluor 488	Thermo Fisher Scientific	Cat#A21202; RRID: AB_141607
Donkey anti-Rabbit IgG- Alexa Fluor 488	Thermo Fisher Scientific	Cat#A21206; RRID: AB_2535792
Donkey anti-Goat IgG- Alexa Fluor 488	Thermo Fisher Scientific	Cat#A11055; RRID: AB_2534102
Streptavidin, Alexa Fluor 488 conjugate	Thermo Fisher Scientific	Cat#S11223

(*Continued on next page*)

Continued

REAGENT or RESOURCE	SOURCE	IDENTIFIER
Donkey anti-Mouse IgG- Alexa Fluor 546	Thermo Fisher Scientific	Cat#A10036; RRID: AB_2534012
Donkey anti-Rabbit IgG- Alexa Fluor 546	Thermo Fisher Scientific	Cat#A10040; RRID: AB_2534016
Donkey anti-Goat IgG- Alexa Fluor 546	Thermo Fisher Scientific	Cat#A11056; RRID: AB_2534103
Donkey anti-Mouse IgG- Alexa Fluor 647	Thermo Fisher Scientific	Cat#A31571; RRID: AB_162542
Donkey anti-Rabbit IgG- Alexa Fluor 647	Thermo Fisher Scientific	Cat#A31573; RRID: AB_2536183
Donkey anti-Goat IgG- Alexa Fluor 647	Thermo Fisher Scientific	Cat#A21447; RRID: AB_2536183
Streptavidin, Alexa Fluor 647 conjugate	Thermo Fisher Scientific	Cat#S32357
Hoechst 33342	Thermo Fisher Scientific	Cat#H1399
Chemicals, peptides, and recombinant proteins		
2-(n-morpholino)ethanesulfonic acid	Dojindo	341–01622
3-Aminopyrrolidine	Sigma Aldrich	540781
4% Paraformaldehyde Phosphate Buffer Solution	FUJIFILM Wako	163–20145
A83-01	FUJIFILM Wako	035–24113
Accutase	Innovative Cell Technologies	AT104
Activin A	R&D	338-AC
Afamin/Wnt3a CM	MBL	J2-001
Arginine vasopressin (AVP)	Sigma Aldrich	V9879
ATRA	Sigma Aldrich	R2625
Bardoxolone methyl	Selleck biotech	S8078
B-27 Supplement minus vitamin A	Thermo Fisher Scientific	12587001
Cell Recovery Solution	BD	354253
CHIR99021	StemRD	CHIR-010
CTS TrypLE Select Enzyme	Thermo Fisher Scientific	A1285901
DAPI	MERCK	10236276001
D-Camphor-10-sulfonic acid	FUJIFILM Wako	037–01032
Dexamethasone	FUJIFILM Wako	041–18861
DiI-conjugated VLDL	Biomedical Technologies, Inc.	BT-922
DMEM/F-12, GlutaMAX	Thermo Fisher Scientific	10565042
DMSO	Sigma Aldrich	D2650
D-PBS(−)	Nacalai Tesque	14249–24
Doxycycline	LKT Labs	D5897
EDTA	Thermo Fisher Scientific	15575020
EGF	R&D	236-EG-01M
Essential 6 Medium	Thermo Fisher Scientific	1516401
FGF1	R&D	231-BC
FGF8	Peprotech	100–25
Forskolin	FUJIFILM Wako	067–02191
Fluvastatin	Abcam	ab120651
GDNF	R&D	212-GD
Geltrex	Thermo Fisher Scientific	A15696-01
Geneticin	Thermo Fisher Scientific	10131035
GFR Matrigel	BD	354230
Hygromycin B	Thermo Fisher Scientific	10687010

(*Continued on next page*)

Continued

REAGENT or RESOURCE	SOURCE	IDENTIFIER
iMatrix-511 silk	Nippi	892021
IWR-1	MERCK	I0161-5MG
KnockOut Serum Replacement	Thermo Fisher Scientific	10828028
LDN193189	Axon Medchem	Axon1509
L-methionine sulfone	FUJIFILM Wako	A17027
Mannitol	Nacalai Tesque	11662–42
Methanol	Nacalai Tesque	21914–03
Normal donkey serum	MERCK	566460
Puromycin	Nacalai Tesque	14861–71
Rapamycin	FUJIFILM Wako	R0161
R-spondin 1	R&D	4645-RS-250
STEM-CELLBANKER GMP grade	ZENOAQ RESOURCE	ZR646
Stem Fit AK02N	Ajinomoto	AK02N
Sucrose	Nacalai Tesque	30403–55
Sunflower oil	Sigma Aldrich	8001-21-6
Tesevatinib	MedChemExpress	HY-13314
Thiazovivin	Santa Cruz	SCB-SC-361380-10
Tolvaptan	Axon medchem	Axon1591
Trimesate	FUJIFILM Wako	26–2340
Triton X-100	Nacalai Tesque	35501–15
TTNPB	Santa Cruz	sc-203303
Venglustat	Selleck biotech	E0646
Y-27632	FUJIFILM Wako	034–24024
Critical commercial assays		
Chromium Next GEM Single Cell 3′ Reagent Kit v3.1	10x Genomics	PN-1000268
Ex Taq	TaKaRa	RR001B
FuGENE6 Transfection Reagent	Promega	E2691
Gateway LR Clonase II Enzyme mix	Thermo Fisher Scientific	11791020
HMT 5 kDa ultrafiltration tube	Human Metabolome Technologies	UFC3LCCNB-HMT
Human 8 × 60K LncRNA expression array	ArrayStar	N/A
In Fusion HD Cloning Kit	TaKaRa	639648
KOD Fx *Neo*	TOYOBO	KFX-201
Lipofectamine Stem Transfection Reagent	Thermo Fisher Scientific	STEM00001
NEBNext Poly(A) mRNA Magnetic Isolation Module	New England Biolabs	E7490
NucleoSpin RNA XS	TaKaRa	740902.5
pENTR™ Directional TOPO Cloning Kits	Thermo Fisher Scientific	K240020SP
ReverTra Ace	TOYOBO	TRT-101
RNeasy Mini kit	Qiagen	74106
SMART-Seq Stranded Kit	TaKaRa	634442
TB Green Premix Ex Taq II	TaKaRa	RR820A
UN-L kit	serotec	A666-00
Wizard SV Gel and PCR Clean-UP System	Promega	A9281
Deposited data		
RNA sequencing data of UBTCs cultured with or without A83-01	This paper	E-GEAD-558
RNA sequencing data of expanded UBTCs	This paper	E-GEAD-559
Single cell RNA sequencing data of CD organoids	This paper	GSE237528

(*Continued on next page*)

Continued

REAGENT or RESOURCE	SOURCE	IDENTIFIER
Single cell gene expression profile of hPSC-derived CD organoids (day 18)	Shi et al., 2022[12]	GSE206153
RNA sequencing data of PKD1$^{+/+}$ UBTCs and PKD1$^{-/-}$ UBTCs	This paper	GSE215875
Microarray data of cyst cells treated with or without TTNPB	This paper	E-GEAD-560
Experimental models: Cell lines		
Human: 585A1 iPSC line	RIKEN BRC	HPS0354
Human: 1231A3 iPSC line	RIKEN BRC	HPS0381
Human: 1383D2 iPSC line	RIKEN BRC	HPS1005
Human: 1383D6 iPSC line	RIKEN BRC	HPS1006
Experimental models: Plasmids		
pHL-EF1a-hcPBase-A	Ishida et al., 2018[19]	N/A
pPV-H1-gRNA-mEF1a-RiH	Ishida et al., 2018[19]	Addgene: 100598
pPV-TetO-SphcCas9-iC-A-EF1a-rtTA-iP	Ishida et al., 2018[19]	Addgene: 100596
PB-TAG-ERN	Kim et al., 2016[55]	Addgene: 80476
Experimental models: Organisms/strains		
Mouse: Pkd1flox/flox: Ksp-Cre	Shibazaki et al., 2008[45]	N/A
Oligonucleotides		
Primers for PCR, see Table S6	This paper	N/A
Software and algorithms		
BZ-X Analyzer	KEYENCE	BZ-X700, BZ-X800
CellRanger v7.0.1	10x Genomics	https://support.10xgenomics.com/
EZR	Kanda. 2013[56]	http://www.jichi.ac.jp/saitama-sct/SaitamaHP.files/statmedEN.html
GeneSpring GX v12.1	Agilent	N/A
MasterHands	Sugimoto et al., 2010[57]	N/A
Monocle v2.22.0	Qiu et al., 2017[58]	http://cole-trapnell-lab.github.io/monocle-release/
Python 3	Python Software Foundation	N/A
Prism 7	GraphPad Software	https://www.graphpad.com/scientific-software/prism/
RStudio	RStudio Team, 2020	N/A
Seurat package v4.1.1	Stuart et al., 2019[59]	http://satijalab.org/seurat/
WinROOF	Mitani Corporation	N/A

RESOURCE AVAILABILITY

Lead contact

Further information and requests for resources and reagents should be directed to and will be fulfilled by the Lead Contact, Kenji Osafune (osafu@cira.kyoto-u.ac.jp).

Materials availability

This study did not generate new unique reagents.

Data and code availability

- The DDBJ accession numbers are E-GEAD-558 and E-GEAD-559 for the RNA-seq data and E-GEAD-560 for the microarray data. The NCBI GEO accession numbers are GSE215875 for the RNA-seq data and GSE237528 for the scRNA-seq data.
- This paper does not report original code.
- Any additional information required to reanalyze the data reported in this paper is available from the lead contact upon reasonable request.

EXPERIMENTAL MODEL AND STUDY PARTICIPANT DETAILS

Animals

All animal experiments were approved by the Institutional Animal Care and Use Committee of the National University Corporation Hokkaido University (No.15-0109) and conducted following guidelines for animal experimentation at Hokkaido University. *Pkd1*$^{flox/flox}$: *Ksp-Cre* mice[45] are a mouse model for ADPKD that massively develop enlarged kidney cysts within a few days after birth. Cre lines were maintained on a heterozygous background as *Pkd1*$^{flox/-}$: *Ksp-Cre*, and *Pkd1* $^{flox/-}$: *Ksp-Cre* mice were crossed with the same mice to generate *Pkd1*$^{flox/flox}$: *Ksp-Cre* mice. All mice were maintained in a temperature-controlled room under a 12 h light-dark cycle. The sex or gender of the mice had no influence or association on the results of this study.

Cell lines

Experiments using human induced pluripotent stem cells (hiPSCs) were approved by the Ethics Committee of the Department of Medicine and Graduate School of Medicine, Kyoto University. Informed consent was obtained from all donors from whom the hiPSCs were derived. Four hiPSC lines, 585A1, 1231A3, 1383D2 and 1383D6, were used. 585A1 was derived from the peripheral blood of a healthy Japanese male in his 30s. 1231A3 was derived from the peripheral blood of a 29-year-old healthy African/American female. 1383D2 and 1383D6 were derived from the peripheral blood of a 36-year-old healthy Asian male. The sex or gender of the cell lines had no influence or association on the results of this study. All hiPSC lines were maintained with feeder-free cultures using StemFit AK02N medium (Ajinomoto) and 0.125 μg/cm^2 iMatrix-511 silk (Nippi). The cells were passaged using 0.5 mM EDTA/PBS solution (Thermo Fisher Scientific) every 4 days and routinely monitored for mycoplasma contamination.

METHOD DETAILS

Directed differentiation

Anterior intermediate mesoderm (AIM) induction

The directed differentiation of hiPSCs into ureteric bud (UB) lineages was described previously.[60] Briefly, undifferentiated hiPSC colonies were dissociated into single cells and plated at a density of 2 × 10^4 cells/cm^2 in 4-well plates (Thermo Fisher Scientific) in StemFit AK02N medium with 10 μM Y-27632 (FUJIFILM Wako) and 0.125 μg/cm^2 iMatrix-511 silk. After 24 h, the cells were washed with pre-warmed PBS and treated with Essential 6 medium (Thermo Fisher Scientific) containing 100 ng/mL Activin A (R&D Systems) and 3 μM CHIR99021 (StemRD). After 16–27 h, the cells were washed with pre-warmed PBS and treated with Essential 6 medium containing 200 ng/mL fibroblast growth factor (FGF) 8 (Peprotech), 0.1 μM 4-[(E)-2-(5,6,7,8-Tetrahydro-5,5,8,8-tetramethyl-2-naphthalenyl)-1-propenyl]-benzoic acid (TTNPB; Santa Cruz Biotechnology), 0.1 μM LDN193189 (Axon Medchem) and 1 μM A83-01 (FUJIFILM Wako) for 2 days. Then, the cells were dissociated into single cells using Accutase (Innovative Cell Technologies), replated at a density of 1.5 × 10^5 cells/cm^2 of Geltrex (Corning)-coated 24-well plates (Greiner Bio-One) in Essential 6 medium containing the same 4 factors plus 10 μM Y-27632, and incubated for an additional 24 h to induce AIM.

Nephric duct (ND) induction

AIM cells were treated with Essential 6 medium containing 1 μM CHIR99021, 0.1 μM LDN193189, 200 ng/mL FGF8, 100 ng/mL glial cell line-derived neurotrophic factor (GDNF; R&D Systems) and 0.1 μM TTNPB for 2 days to induce ND leader cells. To induce epithelialized ND aggregates, ND leader cells were dissociated into single cells after 3-min Accutase treatment at 37°C, seeded onto low-attachment 96-well plates (Sumitomo Bakelite) at a density of 1 × 10^4 cells/well and treated with the same medium and factors plus 10 μM Y-27632 for 2 days.

Branching UB organoid (UBO) induction

Off-target cells were separated from epithelialized ND aggregates by pipetting. The epithelialized ND aggregates were treated with the same medium and factors plus 200 ng/mL FGF1 (R&D Systems), 50 ng/mL EGF (R&D Systems) and 2% Growth Factor Reduced (GFR) Matrigel (Corning) for 6 days to constitute UBOs.

UB tip cell (UBTC) induction

UBOs were treated with Accutase for 5 min at 37°C and subsequently dissociated into single cells by pipetting. The cells were resuspended in DMEM/F12 medium (Thermo Fisher Scientific) containing 2% B-27 supplement minus vitamin A (Thermo Fisher Scientific), 100 ng/mL GDNF, 200 ng/mL FGF1, 0.1 μM TTNPB, 3 μM CHIR99021, 10 μM Thiazovivin (Santa Cruz Biotechnology) and 1 μM A83-01 and seeded onto 48-well plates (Greiner Bio-One) coated with 150 μL hydrogel (in this study, hydrogel was composed of DMEM/F12 medium containing 50% GFR Matrigel and solidified for 1 h at 37°C before use) at a density of 1 × 10^5 cells/well. The medium was changed every 2 days, and the single cells formed UBTC colonies after 7 days.

Expansion of UBTCs

Hydrogel was dissolved with Cell Recovery Solution (Corning) for 30 min at 4°C to detach the UBTC colonies. The UBTC colonies were collected into 15-mL tubes by gentle pipetting with a wide-mouth micropipette (BMBio) so as not to break the colonies and treated with additional Cell Recovery Solution for 30 min at 4°C. Then, the colonies were centrifuged at 500 *g* for 2 min at room temperature and dissociated into single cells after 5-min Accutase treatment at 37°C. The single UBTCs were resuspended in DMEM/F12 medium containing 2% B-27 supplement minus vitamin A, 100 ng/mL GDNF, 200 ng/mL FGF1, 0.1 μM TTNPB, 3 μM CHIR99021, 10 μM Thiazovivin and 1 μM A83-01 (UBTC expansion medium) and replated onto 48-well plates coated with 150 μL hydrogel at a

density of 1 × 10^5 cells/well. The medium was changed every 2 days, and the single UBTCs formed colonies after 7 days. The UBTC colonies were passaged every 7 days.

Cryopreservation

Dissociated ND leader cells and UBTCs were resuspended in STEM-CELLBANKER GMP grade (Nippon Zenyaku Kogyo) at a dilution ratio less than 1 × 10^6 cells/mL. The cell suspension was distributed into cryopreservation tubes at 1 mL/tube. The tubes were frozen for 24 h at −80°C and moved to a liquid nitrogen cell storage tank for long-term cryopreservation. To initiate the cultures, the cells were thawed using a water bath at 37°C.

Reconstitution of CD organoids

The detached UBTC colonies were resuspended in Essential 6 medium containing 10% Afamin/Wnt3a conditioned medium (MBL), 200 ng/mL R-spondin 1 (R&D systems), 0.1 μM LDN193189, 200 ng/mL FGF8, 100 ng/mL GDNF, 0.1 μM TTNPB, 200 ng/mL FGF1, 50 ng/mL EGF, 1 μM A83-01 and 10% GFR Matrigel (CD organoid medium). After pipetting gently with a wide-mouth micropipette, the suspension was distributed to low-attachment 35-mm dishes (Sumitomo Bakelite) at 3 mL/dish. The medium was changed every 3–4 days, and the reconstituted CD organoids were incubated for 14–21 days. To adjust the number of cells in the UBTC aggregates, single UBTCs were resuspended in UBTC expansion medium and seeded onto low-attachment 96-well plates at a density of 5 × 10^3 cells/well. After 2 days, UBTC aggregates were collected into a tube, resuspended in CD organoid medium and distributed to low-attachment 35 mm dishes at 3 mL/dish. The medium was changed every 3–4 days, and reconstituted CD organoids were incubated for 14–21 days.

Further differentiation of CD organoids

To induce principal cells (PCs) and intercalated cells (ICs), CD organoids were treated with Essential 6 medium containing 10% KnockOut Serum Replacement (KSR; Thermo Fisher Scientific), 1 μM IWR-1 (Tocris), 1 μM A83-01, 10 μM Forskolin (FUJIFILM Wako) and 10% GFR Matrigel for 7 days. The medium was changed every 3 days.

Generation of PKD1$^{-/-}$ hiPSCs

To establish PKD1$^{-/-}$ hiPSC lines, we used the CRONUS system.[31] Before transfection, hiPSCs (1231A3 and 1383D2) were plated at a density of 2.5 × 10^4 cells/cm^2 onto 6-well plates (Greiner Bio-One) in StemFit AK02N medium supplemented with 10 μM Y-27632 and 0.125 μg/cm^2 iMatrix-511 silk. After 24 h, the cells were transfected with piggyBac vectors (2 μg each of pPV-TetO-SphcCas9-iC-A-EF1α-rtTA-iP and pPV-H1-gRNA-mEF1α-RiH) and a piggyBac transposase expressing vector (2 μg of pHL-EF1α-hcPBase-A) using FuGENE6 Transfection Reagent (Promega). The gRNA specifically recognizing the PKD1 exon 34 splicing acceptor site was designed as shown in Figure S5A, and pPV-H1-gRNA-mEF1α-RiH was established using an In-Fusion HD Cloning Kit (TaKaRa). One day after the transfection, the cells were treated with 1 μg/mL Puromycin (Nacalai Tesque) and 200 μg/mL Hygromycin B (Thermo Fisher Scientific) for 5 days for drug selection. The expression of gRNA was monitored by the fluorescence of mRFP1. mRFP1-positive colonies were picked and treated with 2 μM Dexamethasone (FUJIFILM Wako) and 1 μM Doxycycline (LKT Labs) to induce gene editing. The mutations of PKD1 gene were confirmed by Sanger sequencing. cDNA was synthesized from total RNA isolated from undifferentiated iPSCs. The sequences of cDNA were also evaluated by Sanger sequencing.

Cyst enlargement and inhibition of cyst formation

For cyst enlargement, cyst-containing CD organoids were treated with CD organoid medium containing 10 μM forskolin for 2–5 days. To inhibit cyst formation, 4-week-cultured 1383D2-PKD1$^{-/-}$ UBTCs were expanded by adding 1 μM fluvastatin (Abcam) for 7 days. The fluvastatin-treated UBTCs were dissociated into single cells and resuspended with UBTC expansion medium to form UBTC aggregates. Then, the reconstitution of CD organoids was performed as described above.

Expansion of cyst cells

The cyst structures mechanically separated from CD organoids were dissociated into single cells by pipetting after 3-min treatment with a 1:1 TrypLE (Thermo Fisher Scientific)/Accutase solution at 37°C. The cells were resuspended with DMEM/F12 medium containing 2% B-27 supplement minus vitamin A, 10% Afamin/Wnt3a conditioned medium, 200 ng/mL R-spondin 1, 200 ng/mL FGF1 and 10 μM Y-27632 (Cyst expansion medium) and seeded onto 48-well plates coated with 150 μL hydrogel at a density of 5 × 10^4 cells/well. The medium was changed every 3 days, and the single cells formed cyst structures after 10 days. For the passage culture of cysts, hydrogel was dissociated after 30-min treatment with Cell Recovery Solution at 4°C to detach day-10 cyst structures. Cyst structures were collected into 15-mL tubes by gentle pipetting with a wide-mouth micropipette so as not to break the cysts and treated with additional Cell Recovery Solution for 30 min at 4°C. Then, the cysts were centrifuged at 500 *g* for 2 min at room temperature and dissociated into single cells after 3-min treatment with a 1:1 TrypLE/Accutase solution at 37°C. The single cyst cells were resuspended with Cyst expansion medium and seeded onto 48-well plates coated with 150 μL hydrogel at a density of 5 × 10^4 cells/well to reconstitute cyst structures.

HTS platform

To generate cyst cells, we induced cyst-containing CD organoids from cryopreserved 6-week-cultured UBTCs derived from PKD1$^{-/-}$1383D2-hiPSCs. Then, we mechanically detached cysts from the organoids and enzymatically dissociated them into single cyst cells (primary cyst cells). These cells were resuspended with Cyst expansion medium and seeded onto 24-well plates coated

with 250 μL hydrogel (50% GFR Matrigel) at a density of 1 × 10^4 cells/well. After 10 days of expansion culture, reconstituted cysts were collected using Cell Recovery Solution and enzymatically dissociated into single cyst cells (secondary cyst cells). To accelerate the reconstitution of the cyst structures from single cyst cells, primary or secondary cyst cells were suspended in 100 μL Cyst expansion medium containing 10 μM forskolin, seeded onto 96-well plates (CellCarrier Ultra or PhenoPlate; PerkinElmer) coated with 35 μL hydrogel (50% GFR Matrigel) at a density of 1 × 10^4 cells/well and cultured for 2 days. To promote cyst enlargement, 2.5 μM arginine vasopressin (AVP; Sigma-Aldrich) was added to the Cyst expansion medium during the cyst reconstitution process. Then, the medium was changed to 100 μL of DMEM/F12 medium containing 2% B-27 supplement minus vitamin A, 2.5 μM AVP, 200 ng/mL FGF1 and each target compound. The target compounds were diluted in DMSO to generate 1–10 μM stocks, and 1 μL of each diluted compound or DMSO was added to 99 μL of DMEM/F12 medium containing 2% B-27 supplement minus vitamin A, 2.5 μM AVP and 200 ng/mL FGF1 to achieve a final concentration of the desired concentration and incubated for 3–4 days. Three images in each well were taken by z stack imaging at 4× magnification using a BZ-×800 (KEYENCE), and image cytometer analysis was performed using a BZ-X Analyzer (KEYENCE). To accurately measure the area of the cysts, the evaluation was performed excluding cell clumps smaller than 2,000 μm^2 and cysts over the edge of the image. We averaged the size of 200–300 cysts per compound to minimize the effects of variations in individual cyst size. Target compounds, including 1 μM venglustat (Ibiglustat; Selleck biotech), 0.1 μM bardoxolone methyl (Selleck biotech), 1 μM tesebatinib (MedChemExpress), 1 μM fluvastatin, 1 μM rapamycin (FUJIFILM Wako), 0.1 μM TTNPB and 0.1 μM ATRA (Sigma-Aldrich), were evaluated using 0.1% DMSO and 5 μM tolvaptan (Axon Medchem) as the negative and positive control, respectively. The total number of cysts used for evaluation in this study are shown in Table S5.

Overexpression of CDKN2B in cyst cells

To generate the entry clone containing kozak sequence with cDNA sequence of CDKN2B, the sequence was amplified by PCR (TOYOBO) from a template of cDNA generated from 1383D2-PKD1$^{-/-}$ cyst cells. The PCR fragment was purified using Wizard SV Gel and PCR Clean-Up System (Promega) and cloned into pENTR/D-TOPO vector (pENTR Directional TOPO Cloning Kit; Thermo Fisher Scientific). The target sequence was transferred from the entry vector to the destination vector (PB-TAG-ERN; addgene) by the LR Gateway reaction (Thermo Fisher Scientific) using standard protocols. To establish doxycycline-inducible CDKN2B-expressing hiPSCs, we used the piggyBac system. Before transfection, 1383D2-PKD1$^{-/-}$ hiPSCs were plated at a density of 2 × 10^4 cells/cm^2 onto 6-well plates (Greiner Bio-One) in StemFit AK02N medium supplemented with 10 μM Y-27632 and 0.125 μg/cm^2 iMatrix-511 silk. After 48 h, the cells were transfected with a piggyBac vector (1 μg of PB-TAG-ERN containing kozak-CDKN2B) and a piggyBac transposase expressing vector (1 μg of pHL-EF1α-hcPBase-A) using Lipofectamine Stem Transfection Regent (Thermo Fisher Scientific). Two days after the lipofection, the cells were treated with 50 μg/mL Geneticin (Thermo Fisher Scientific) for 5 days for drug selection. Six colonies were picked and induced into the cyst structures. Then, the isolated single cyst cells were plated onto 50% Matrigel-coated 48-well plates. After 2-day culture, the cysts were treated with or without 1 μM doxycycline to induce CDKN2B expression. The line with the highest CDKN2B expression efficiency was used to evaluate the effects of CDKN2B overexpression on cyst enlargement.

RT-PCR and quantitative RT-PCR

Total RNA was isolated using an RNeasy Kit (Qiagen) according to the manufacturer's recommendations, followed by cDNA synthesis using standard protocols. Briefly, cDNA was synthesized from 100 ng of total RNA using ReverTra Ace (TOYOBO). The cDNA samples were subjected to PCR amplification using a thermal cycler (Veriti 96-well Thermal Cycler; Applied Biosystems). PCR was performed using the Ex-Taq PCR Kit (TaKaRa) according to the manufacturer's instructions. Quantitative RT-PCR was performed using TB Green Premix Ex Taq II (TaKaRa). The expression of each gene was normalized to the level of βACTIN expression.

Flow cytometry analysis

UBOs and UBTCs were treated with 10 μg/mL DiI-conjugated VLDL (Biomedical Technologies, Inc) for 2 h at 37°C. Then, the cells were dissociated into single cells by pipetting after 3-min Accutase treatment at 37°C. After washing with DMEM/10% FBS, the cells were resuspended with PBS. Dead cells stained with 4′, 6-Diamidino-2-phenylindole, dihydrochloride (DAPI; 1 μg/mL; Thermo Fisher Scientific) were excluded from the analysis. Single cells were analyzed using a FACS Aria II (BD). Cells derived from UBOs and UBTCs without DiI-VLDL treatment were used as negative controls for gating. For the proliferation and apoptosis cell rate analysis, single cyst cells were fixed with ice-cold 70% methanol for 10 min at 4°C. After washing with PBS, the fixed cells were blocked with 0.5% BSA/2% FBS/PBS (blocking solution) for 5 min at room temperature. Primary antibodies were diluted in blocking solution at 1:100 and incubated for 15 min at room temperature. After washing with PBS, the cells were incubated with secondary antibodies diluted with blocking solution at 1:500 for 15 min at 4°C. Then, the filtered samples were analyzed using the FACS Aria II. Cells with isotype control antibody treatments were used as negative controls for gating.

Bulk RNA sequencing analysis

RNA sequence library preparation, sequencing, mapping and gene expression analysis were performed by DNAFORM. Qualities of total RNA were assessed by a Bioanalyzer (Agilent Technologies) to ensure that the RNA integrity number was over 7.0. After poly (A) + RNA enrichment by NEBNext Poly (A) mRNA Magnetic Isolation Module (New England BioLabs), double-stranded cDNA libraries (RNA-seq libraries) were prepared using SMARTer Stranded Total RNA Seq Kit v2 Pico Input Mammalian (Clontech)

according to the manufacturer's instructions. RNA-seq libraries were sequenced using paired end reads (50 nt of read1 and 25 nt of read2) on a NextSeq 500 instrument (Illumina). Obtained reads were mapped to the human GRCh38 genome using STAR (version 2.7.2b) or Hisat2 (version 2.1.0). Reads on annotated genes were counted using featureCounts (version 1.6.1). FPKM and TPM values were calculated from mapped reads by normalizing to total counts. Differentially expressed genes (DEGs) were detected using the DESeq2 package (version 1.26.0). The list of DEGs detected by DESeq2 was used for the GSEA. Heatmaps and volcano plots were created using the bioinfokit package (version 2.0.1).

Single cell RNA-sequencing

For single cell RNA-sequencing, CD organoids generated from 2- and 6-week-cultured UBTCs were extracted from 10% Matrigel using Cell Recovery Solution on ice for 10 min. After aspirating Cell Recovery Solution, the organoids were washed once with PBS and incubated in Accutase for 5 min at 37°C. The dissociated single cells were resuspended with 0.04% BSA/PBS at a density of 1×10^3 cells/μL, passed through a 40-μm strainer (Corning) and followed by library preparation using the Chromium Single Cell 3′ Reagent Kit v3.1 (PN-1000268; 10x Genomics) and the Chromium Controller (10X Genomics) according to manufacturer's instructions. The library was sequenced on a DNBSEQ-G400 (MGI). From fastq files, quality control, alignment to reference genome (hg38) and generation of count tables were done using CellRanger v7.0.1 (10x Genomics). Dimensionality reduction was carried out using the Uniform Manifold Approximation and Projection (UMAP) algorithm, and the cell clusters were visualized using Seurat package v4.1.1. Genes with adjusted p-values <0.05 and log2foldchange >0.25 based on the Tukey-Kramer test were considered DEGs. For reference-based mapping, we uploaded the datasets representing each CD organoid as an R object to the human kidney application on the Azimuth web app (https://azimuth.hubmapconsortium.org). In the Azimuth toolkit, we referred to reported gene expression patterns[26] to decide the list of marker genes used to define each CD cluster. A pseudotime trajectory analysis was performed with R package monocle v2.22.0. The DDRTree method was utilized for dimension reduction and cell ordering along the pseudotime trajectory. Genes used for the pseudotime heatmap were taken from the first 1,000 DEGs (by *P*). Enrichment analysis was performed using the Metascape bioinformatics tool.

Microarray analysis

Microarray analysis was performed by Filgen using a Human 8 × 60K LncRNA expression array (ArrayStar) to globally profile human protein-coding transcripts. Sample labeling and array hybridization were performed according to the Agilent One-Color Microarray-Based Gene Expression Analysis protocol (Agilent Technology). Data were collected using Agilent's Feature Extraction software. Raw signal intensities were normalized using the quantile normalization method in GeneSpring GX v12.1. Low intensity mRNAs were filtered. mRNAs for which at least 3 out of 6 samples had flags in Present or Marginal were chosen for further analysis. Differentially expressed mRNAs between two groups with statistical significance were passed using Volcano filtering.

Metabolome analysis

Metabolome analysis was performed as described previously.[61] Briefly, 1×10^6 UBTCs were washed twice with cold 5% mannitol (Nacalai tesque), and 1 mL ice-cold methanol (Nacalai tesque) with internal standards (25 μM each of L-methionine sulfone (FUJIFILM Wako), 2-(n-morpholino)ethanesulfonic acid (Dojindo) and D-Camphor-10-sulfonic acid (FUJIFILM Wako)) was applied for the metabolome extraction. 400 μL extract was mixed with chloroform (400 μL) and distilled water (200 μL) and centrifuged at 10,000 *g* for 3 min at 4°C. For capillary electrophoresis time-of-flight mass spectrometry (CE-TOFMS), 400 μL of aqueous layer was filtered with an HMT 5 kDa ultrafiltration tube (Ultrafree-MC-PLCC for Metabolome Analysis; Human Metabolome Technologies) to remove proteins and centrifuged at 9,100 *g* for 2.5 h at 20°C. The filtrate was dried using an evacuated centrifuge for 2 h at 40°C. The product was dissolved in 25 μL distilled water containing 200 μM 3-Aminopyrrolidine (Sigma-Aldrich) and 200 μM Trimesate (FUJIFILM Wako). Samples were dissolved in distilled water, and CE-TOFMS (Agilent Technologies) was performed according to previous studies.[61,62] For liquid chromatography quadrupole TOFMS (LC-QTOFMS), 600 μL methanol containing 1 μM reserpine was added to the residue of the above filtrated extract and mixed for 10 min. After centrifugation at 10,000 g for 20 min at 20°C, 400 μL supernatant was transferred to a sample vial. Samples were analyzed by LC-QTOFMS (Agilent Technologies). The LC system was the Agilent 1290 Infinity HPLC (Agilent Technologies, Palo Alto, CA). This system was equipped with an automatic degasser, binary pump, thermostated column compartment, and autosampler. Chromatographic separation was performed using an Acquity UPLC HSS T3 C18 column (2.1 i.d. × 50 mm, 1.8 μm; Waters, Milford, MA), and the column temperature was maintained at 45°C. The mobile phase consisted of acetonitrile-methanol-water (3:1:1), with 5 mM ammonium formate as eluent A and isopropanol with 5 mM ammonium formate as eluent B. The initial mobile phase was 100% eluent A at a flow rate of 0.3 mL/min. The gradient profiles of eluent B were 40%, 64%, 64%, 82.5%, 85%, and 95% at 5, 7.5, 12, 12.5, 19, and 20 min, respectively. The injection volume was 5 μL. MS data were acquired from a 6530 Accurate-Mass Q-TOF mass spectrometer using the dual ESI of G3251A (Agilent). Samples were analyzed by both positive and negative ion electrospray MS. The MS condition was as follows: drying gas 10 L/min at 350°C, nebulizer 55 psig, capillary voltage 3,500 V, fragmentor 150 V, skimmer 90 V, OCT1 RF Vpp 500 V, and scan range *m/z* 100-1,700. Lock masses were as follows: TFA at *m/z* 112.9856 and HP-0921(+TFA) at *m/z* 1033.9881 in negative-ion mode and purine at *m/z* 121.0509 and HP-0921 at *m/z* 922.0098 in positive-ion mode. Peaks detected by CE-TOFMS and LC-QTOFMS were extracted using automatic integration

software (MasterHands)[57] to obtain peak information, including m/z, migration time (MT) and peak area. Metabolite concentrations were calculated by normalizing the peak area of each metabolite with respect to the area of the internal standard and by using standard curves.

ATRA treatment

Pkd1$^{flox/flox}$: *Ksp-Cre* mice (cystic) and *Pkd1*$^{flox/-}$ mice (non-cystic) were intraperitoneally injected with 5 or 10 mg/kg mouse body weight of ATRA diluted with 2% DMSO and sunflower oil (Sigma-Aldrich) or vehicle alone at three days of age. Mice were sacrificed at nine days of age after being anesthetized, and tissue and blood samples were obtained.

Blood sample measurements

Blood samples were withdrawn from the right atrium after being anesthetized, and serum was separated and frozen at −80°C until measurements were taken. Blood urea nitrogen (BUN) was measured using the UN-L Kit (Serotec) according to the manufacturer's instructions.

Histology and cystic index determination

For histology, kidneys were obtained by perfusion fixation in 4% paraformaldehyde (PFA). Paraffin-embedded kidney sections were cut at 4-μm thickness, deparaffinized, and stained with hematoxylin and eosin according to standard protocols. Images of hematoxylin and eosin-stained sections were obtained using bright-field microscopy. The cystic index was defined as (total cystic area/total tissue area) × 100 (%) and measured using morphometric software (WinROOF, Mitani Corporation).

Immunostaining

Immunostaining was performed as described previously.[10] For frozen sections, samples were fixed with 4% PFA/PBS (FUJIFILM Wako) for 1 h at 4°C. Fixed samples were washed with PBS, treated with 30% sucrose (Nacalai tesque)/PBS and frozen with OCT compound (Tissue-Tek) to make frozen sections by cryosectioning. The frozen sections were washed with distilled water and blocked with 1% normal donkey serum (MERCK) and 3% bovine serum albumin (BSA; Nacalai tesque)/PBT (PBS/0.25% Triton X-100, Nacalai tesque) (blocking solution) for 1 h at room temperature. Primary antibodies were diluted in blocking solution at 1:500 and incubated overnight at room temperature. After washing with PBS, the sections were incubated with secondary antibodies diluted with blocking solution at 1:500 for 1 h at room temperature. Then, the sections were washed with PBS, and fluorescence images were captured by a BZ-X700 (KEYENCE) or BZ-X800 (KEYENCE). Image analysis was performed using a BZ-X Analyzer (KEYENCE). An FV3000 confocal laser scanning microscope (OLYMPUS) was used to image the cilia and to obtain high resolution and magnification images.

QUANTIFICATION AND STATISTICAL ANALYSIS

Data are expressed as the mean ± s.d., and statistical analysis was performed using EZR[56] or GraphPad Prism version 7 for Windows. Student's t test, Chi square test, Mann-Whitney U test and one-way ANOVA with Tukey's test were used for the assessments. p-values lower than 0.05 were considered significant.